Aerodynamic Performance Analysis of Different Distributed Electric Propulsion Configurations with Low-Fidelity Models

Master Thesis Report

Matic Tomaževič

Delft University of Technology

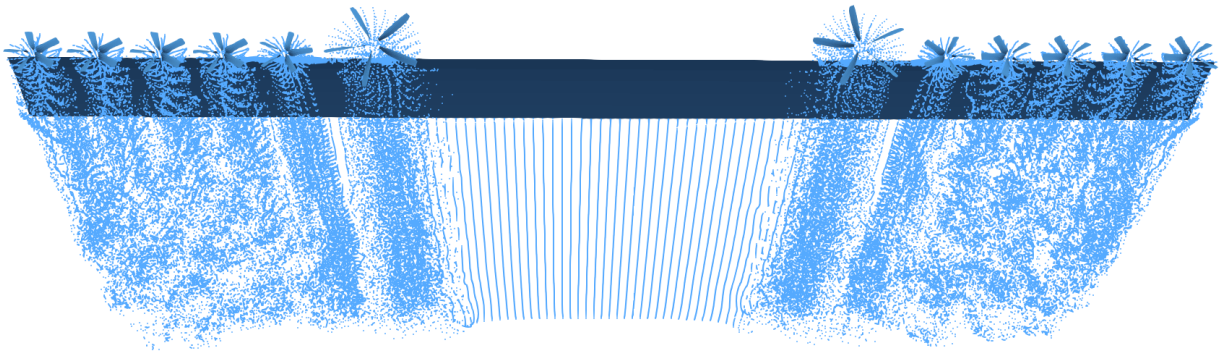

TU Delft

Aerodynamic Performance Analysis of Different Distributed Electric Propulsion Configurations with Low-Fidelity Models

Master Thesis Report

by

Matic Tomaževič

to obtain the degree of Master of Science

at the Delft University of Technology,

to be defended publicly on Monday March 31, 2025 at 11:00 AM.

Student number:	5850347	
Project duration:	March, 2024 – March, 2025	
Thesis committee:	Dr. ir. W. J. Baars	TU Delft, chair
	Dr. F. Oliviero,	TU Delft, responsible thesis supervisor
	D. Eržen,	Pipistrel Vertical Solutions, company supervisor
	Dr. ir. T. Sinnige,	TU Delft, examiner

Cover:	A DEP configuration modelled in DUST
Style:	TU Delft Report Style, with modifications by Daan Zwaneveld

TU Delft

Preface

The following report is a result of a year-long master thesis research project at Delft University of Technology, done in collaboration with Pipistrel Vertical Solutions. As one of the leading companies in the sector of electric aviation, Pipistrel is also putting some focus on the research of Distributed Electric Propulsion (DEP) systems and this project is one of the first steps in that direction.

For me, distributed electric propulsion is a fascinating topic which would potentially revolutionize the way we think about aircraft design. To be at the forefront of its research with Pipistrel and TU Delft is a tremendous opportunity and I am grateful for the chance to work on this project. I would like to thank my supervisors, Dr. ir. Fabrizio Oliviero and David Eržen for their guidance and support throughout the project. Their expertise and knowledge have been invaluable in the development of this research. I would also like to thank the entire Flight Physics department at Pipistrel for giving me the opportunity to work on this project and for providing me with the necessary resources and support. I would also like to thank my girlfriend Špela, my family and friends for their support and encouragement throughout the project.

This project has been quite a challenge but also a great learning experience. I have learned a lot about the topic of distributed electric propulsion, aerodynamics, and aircraft design in general. I hope that this report will be a valuable contribution to the research in this field and that it will inspire others to continue exploring the possibilities of distributed electric propulsion.

Matic Tomaževič
Delft, March 2025

Summary

This thesis investigates the aerodynamic performance of various Distributed Electric Propulsion (DEP) configurations using low-fidelity modeling tools. The study is motivated by the growing interest in sustainable aviation and the potential of DEP systems to offer improved aerodynamic efficiency, reduced noise, and greater design flexibility. Conducted in collaboration with Pipistrel Vertical Solutions, the research focuses on evaluating and optimizing different DEP layouts that combine minimum induced loss (MIL) propellers, dedicated for efficient cruise, and lift-augmenting (LA) propellers, designed to enhance lift during take-off and landing.

A key objective of the work is to develop a computationally efficient optimization framework suitable for early-stage design, capable of assessing multiple DEP configurations. To that end, the study integrates propeller design methodologies, slipstream modeling, and a DEP-specific lifting line solver into a single low-fidelity analysis tool. This framework is then coupled with multi-objective optimization algorithms, such as NSGA-II and SMPSO, to explore a wide design space and identify configurations that minimize take-off distance and cruise power requirements.

The thesis compares three main DEP arrangements, varying the number, size, and spanwise placement of MIL and LA propellers. The results show how propeller positioning and interaction effects influence overall aerodynamic performance, and they highlight the value and limitations of low-fidelity models in capturing these phenomena. The insights gained provide a foundation for future development of DEP systems and for refining low-fidelity tools for preliminary aircraft design.

Contents

Nomenclature

Abbreviations

Abbreviation	Definition
BEMT	Blade Element Momentum Theory
DEP	Distributed Electric Propulsion
LA	Lift-Augmenting (Propeller)
MIL	Minimum Induced Loss (Propeller)
SRF	Swirl Recovery Factor
STOL	Short Take-Off and Landing
VTOL	Vertical Take-Off and Landing

Symbols

Symbol	Definition	Unit
a	axial induction factor	
a'	tangential induction factor	
B	number of blades	
c	airfoil section chord length	[m]
c_d	sectional drag coefficient	
C_D	(total) drag coefficient	
C_{D_i}	induced drag coefficient	
c_l	sectional lift coefficient	
C_L	(total) lift coefficient	
C_T	thrust coefficient	
F	Prandtl tip loss factor	
J	advance ratio	
p	pressure	[Pa]
P	power	[W]
Q	torque	[Nm]
r	propeller radial station	[m]
R	propeller radius	[m]
T	thrust	[N]
T_C	thrust coefficient based on the free stream dynamic pressure	
v_a	induced axial velocity	[m/s]
v_t	induced tangential (swirl) velocity	[m/s]
V	velocity	[m/s]

Symbol	Definition	Unit
V_∞	free stream velocity	[m/s]
α	angle of attack	[°, rad]
α_i	induced angle of attack	[°, rad]
β	twist angle	[°, rad]
Γ	circulation	[m^2/s]
ρ	density	[kg/m^3]
ϕ	inflow angle	[°, rad]
σ	propeller solidity	
ω	angular velocity	[rad/s]
Ω	propeller rotation rate	[rad/s]

1

Introduction

With the electrification of the aviation sector, we will likely see an increase in the number of propeller-powered aircraft. This will happen due to the fact that turboprop propulsion system was found to be up to 30% more efficient than an equivalent turbofan one below Mach numbers of 0.7 (Veldhuis, 2005). As propellers are the first means of propulsion that were used on airplanes and thus are not a novel invention, they were the subject of a lot of different research in the past, mostly regarding their design and interaction with other parts of the aircraft. However, we are already observing the influence of side benefits of electrification, some of which include scalability and modularity of electric propulsion systems, which enable us to create novel aircraft configurations that could bring some welcome improvements over the traditional configurations. At this point, it is thus important to re-examine some aspects of propeller design and look at them in a new light since they could be crucial in designing an efficient distributed electric propulsion (DEP) system.

At least on paper, DEP configurations offer several advantages over the traditional configurations. Firstly, by distributing the propulsion over a wider spanwise distance, more of the wing area is blown by the propellers, thus increasing the area with higher dynamic pressure and the lift generated by the wing. This is especially important for low-speed flight, where maximizing lift is crucial. Secondly, installing inboard-up rotating propellers, which rotate in the opposite direction of the wing tip vortex, towards the tip of the wing, can help to counteract said vortex and decrease the induced drag, which is the main source of drag at low speeds (Anderson, 2010). Thirdly, due to an increased number of propellers, the redundancy of the propulsion system is increased, which is important for the safety of the aircraft. Lastly, DEP configurations give the possibility of having dedicated propellers for different stages of flight, which can help in increasing the efficiency of the aircraft and reduce noise pollution.

This thesis was written in collaboration with Pipistrel, one of the leading companies in the field of sustainable aviation, and since DEP certainly falls within its scope, it is natural that they are interested in this topic. In the past, they have participated in the Unifier19 project together with TU Delft and Politecnico di Milano, where a concept of a 19-seater hydrogen fuel cell-powered DEP commuter aircraft was being developed. From it, the DEP configuration looked into in this thesis was derived. It features either one or two propellers (depending on the configuration) designed for cruise conditions following the minimum induced loss (MIL) principle which will

be the only propellers operating during cruise with efficiency in mind. Mounted alongside will also be *N* lift-augmenting (LA) propellers, whose main purpose is to increase the effective lift during take-off and landing phases of the flight. During the cruise phase, their blades could stow away as the need for lift and thrust during this phase lower. Furthermore, propellers on aircraft that have one or two of them, are often dimensioned for the take-off and landing phases of the flight as they are the most demanding, which means that they might be oversized for the cruise phase and thus not as efficient as they could be. By having dedicated lift-augmenting propellers and a dedicated cruise propeller, the efficiency of the propulsion system in each stage of flight can be increased.

Hopefully, by the end of this thesis, a better understanding will be gained into how different DEP configurations compare to traditional configurations and how they can be optimized to achieve the best performance.

1.1 Scope of the Thesis

The focus of this study was to compare different propeller configurations for a DEP system. This includes three different positions of the MIL propeller, various numbers of the LA propellers and numerous propeller sizes and positions with respect to the wing. This was achieved by developing an optimization procedure that could be used in the early stages of a DEP aircraft design. It utilizes lift-augmenting and minimum induced loss propeller design procedures, a propeller slipstream evaluation procedure, and a DEP-specific lifting line solver. The aim of this research was not to produce the best design for a DEP aircraft but rather to see how different propeller configurations influence its aerodynamic performance.

Because most optimization cases require a high number of solutions to be evaluated, it is beneficial for the evaluation function to be computationally cheap. For this reason, low-fidelity tools, such as the lifting line analysis or vortex-lattice analysis, are much more suited for this task than high-fidelity tools, such as CFD. However, they can be computationally less expensive because they are based on assumptions and simplified models that might not always be accurate. It is thus important that these assumptions and models are presented, well understood, and kept in mind throughout the research. The theory and their implementation will be presented in the following chapters.

It is also important to acknowledge that this thesis does not focus on aircraft design and its goal is not to present a particular DEP configuration. Aircraft design is a highly complex subject, involving many different disciplines, which cannot all be taken into account in a single thesis work. Rather, the present work deals with different DEP design procedures from an aerodynamic and propulsive efficiency point of view, which also includes analyzing few selected and generated DEP configurations. It will not take into account the stability, weight, cost, safety, noise, and other factors that are also very important when designing an aircraft. Emphasis will be put on minimizing the take-off distance and power required during the cruise phase of the flight as these are of the main selling points of the DEP configurations. Other aspects of a full DEP aircraft design procedure will have to be looked at in future research.

The DEP configurations considered in this thesis consisted of multiple propellers in a tractor configuration. Specifically, three potential options were defined: 1) designs with one MIL propeller on the inboard side of each wing and *N* lift-augmenting propellers distributed outboard

up to the wing-tips, 2) designs with one MIL propellers on the tips of the wing with *N* lift-augmenting propellers distributed inboard, 3) and finally a design with one MIL propeller mounted on the tail of the aircraft and *N* lift-augmenting propellers situated in front of the wing. There are, of course, many other possibilities for positioning the propellers, either on the wings or somewhere else along the fuselage (nose, tail, rear side of the fuselage). However, in the present work, these three configurations were chosen because they were deemed most interesting and viable to be potentially implemented on a DEP aircraft in the future. By comparing these configurations and optimizing different propeller size and position parameters, an insight into their effect on aircraft performance and efficiency both during the climb and cruise stages of flight will be gained.

1.2 Research Question

The research question that this thesis aims to answer is:

How do aircraft with different distributed electric propulsion configurations compare to aircraft with traditional propeller configurations in terms of propulsive and aerodynamic efficiency?

- *How do propeller positions and the number of propellers influence the performance of DEP configurations?*
- *Can an aircraft with a DEP configuration of Unifier19, consisting of one or two minimum induced loss propellers and N lift-augmenting propellers, be more efficient than a traditional configuration with one or two propellers?*
- *To what degree can low-fidelity tools, such as the lifting line method, accurately predict the performance of DEP configurations?*

By answering these questions, a better understanding of the potential of DEP configurations can be obtained and the limitations of low-fidelity tools in predicting their performance can be better understood. This knowledge can be used to further develop DEP configurations and to improve the tools used to design them.

1.3 Thesis Outline

The body of the present work will firstly review the literature and lay down the groundwork for the research process. Initially, the most relevant theory of lifting surface and isolated propeller modelling will be presented, followed by the interaction effects between a wing and a propeller mounted in front of it. Because it is impossible to model this interplay exactly, especially when using low-fidelity tools, only the most influential effects will have to be modeled and for this reason, it is important to understand them. Next, the theory behind lift-augmenting and minimum induced loss propellers will be presented, followed by a short introduction to optimization algorithms.

The following chapter will first present the methodology and tools used for designing and evaluating MIL and LA propellers. They will further be compared against one another to verify the theory and analyze their performance. A slipstream model for a general blade loading will be presented which can predict the axial velocity profile anywhere inside the slipstream.

Next, in a section about DEP design and evaluation the setup of a DEP-specific lifting line solver will be presented. Its accuracy will be verified against literature. In the end, different DEP configurations will be analyzed in order to see how some design variables affect the aircraft take-off distance.

In chapter 5 it will be presented how the lifting line solver was coupled with two optimization algorithms and an objective function that minimizes take-off distance and cruise power was set up. The correlation between different input variables and the objectives will be analyzed and the general trends of the optimization results will be presented. The obtained designs were also recreated in a mid-fidelity tool called DUST in order to validate the optimization results. In the last chapter, a conclusion of the entire work done will be presented.

2

Literature Study

2.1 Lifting Surface Aerodynamics Modelling

Lifting surfaces are a part of most aerodynamic devices whose main purpose is to generate lift or thrust, including wings and propellers which are being designed and evaluated in the present work. Their geometry creates a pressure difference between the top and bottom surfaces, which results in a lift force. There are many different ways of modelling the aerodynamics of lifting surfaces, ranging from simple 2D models, which can include different levels of corrections, to complex 3D models.

One of the simplest ways to model the aerodynamics of a lifting surface is by using thin airfoil theory. Its main equation was presented in Munk's PhD thesis in (1909), however the groundwork of airfoil aerodynamics was laid out by his mentor Ludwig Prandtl. The theory assumes that an airfoil can be represented by its mean camber line, making it thin. A number of vortex sheets with unknown strength are placed along its length and their strength is determined by the flow tangency and the Kutta conditions. Later, Munk presented a theory that extends the thin airfoil theory to simple thin wings (Munk, 1923).

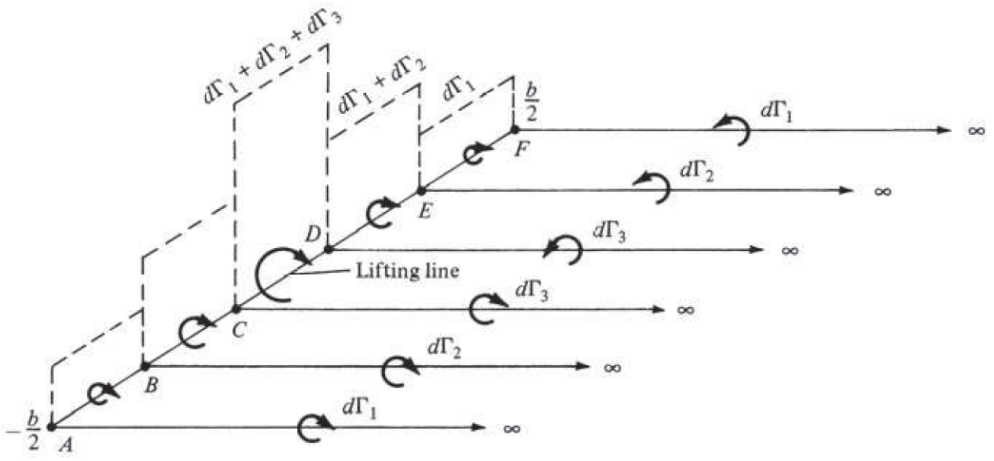

Figure 2.1: Prandtl's lifting line model with three horseshoe vortices. Image taken from Anderson (2010).

The lifting line theory, developed by Ludwig Prandtl (1923), is the first theory for modelling finite wings. It assumes that a lifting surface can be represented by a series of horseshoe vortices with the bound vortices coinciding on the lifting line and with two trailing vortices on each side of every horseshoe vortex which induce downwash and stretch to infinity. The idea and the theory is rather simple, however many different ways of numerically evaluate it were developed. The classical way of solving the lifting line problem is by representing the circulation using sine functions and utilizing the Fourier sine analysis to find the Fourier coefficients. The Weissinger Theory (1947) models a finite wing like a simple panel method with one chord-wise element. It extends the classical lifting line theory by adding a control point at three-quarter chord position and enforcing flow tangency at that location. This way of discretization poses a number of advantages over the classical lifting line theory, mainly that it allows for the analysis of swept and lower aspect ratio wings, more accurate prediction of non-elliptic wing performance and more flexibility in the placement and number of the control points. An extensive study comparing the two was done by Baldoino and Bodstein (2004). For more accurate induced drag prediction the Trefftz method can be used, which calculates it using momentum conservation and vorticity distribution on the Trefftz plane infinitely downstream of the wing instead from the circulation distribution (Kroo, 1986). Furthermore, many methods for unsteady lifting line theory were developed, like the one by Devinant (1998).

By adding more chord-wise horseshoe vortices and control points to the Weissinger's extended lifting line method (ELLM), a vortex lattice can be created. It has all of ELLM's benefits, however it allows for 3D geometries (cambered lifting surfaces) to be modelled. This also results in chord-wise discretization alongside spanwise discretization. Other common lifting surface aerodynamic models also include the panel method, developed by Hess and Smith (1967), which can predict potential flow around any 3D geometry, and different Reynolds-Averaged Navier-Stokes (RANS) CFD models.

The goal of this thesis is to analyze a big design space like it would be done in the beginning of a DEP design project. This includes evaluating many different DEP configurations and assessing their performance according to some function. Because of this, high-fidelity tools, such as CFD simulations, are not appropriate, since they require large amounts of computation power and time, therefore low-fidelity methods, e.g. the lifting line of the vortex lattice methods are much better suited for this purpose. One way to analyze the entire design space is to randomly sample it and evaluate the selected designs, however this is relatively time intensive. By wrapping the evaluation function in an algorithm that can analyze the entire design space, distinguish between good and bad performing designs, converge towards regions in the design space that output better solutions and ultimately output superior ones, the regions with more relevant results can be searched in much more detail without wasting precious resources in other parts of the design space. Such algorithms are called optimization algorithms and are described in section 2.6.

In summary, various methods exist for modeling the aerodynamics of lifting surfaces, each with its own advantages and limitations. The choice of method depends on the specific requirements of the analysis, such as the level of accuracy needed, computational resources available, and the complexity of the geometry being studied.

2.2 Isolated Propeller Aerodynamics

Because direct modelling of propeller-wing interaction effects can be computationally too expensive, it is common to first evaluate the aerodynamics of an isolated propeller (Jameson, 1970). The most common approaches are the momentum theory, blade element momentum theory, utilization of lifting lines or vortex lattices to model propeller blades, and CFD simulations.

Propeller is a device used to produce thrust and propel an aircraft forward or keep a helicopter or a VTOL airborne. In essence, they are a just a collection of rotating lifting surfaces producing lift and drag forces. The resultant of these forces in the direction of the propeller rotation axis is called thrust while the moment in the plane of rotation trying to slow the propeller down is called torque. Because a propeller blade is just a lifting surface, it too forms a tip vortex and a trailing vortex sheet. The combination of these effects from all blades is called a helical vortex sheet.

One of the most common procedure for designing a propeller is the so called Minimum Induced Loss (MIL) procedure. It is based on the theory of Prandtl and Betz (1919), which states that an elliptic load distribution of a wing will produce a uniform downwash and a "rigid" vortex sheet which would impart the least kinetic energy on the flow field and thus minimum losses. In a similar manner an analytic solution for a propeller blade circulation distribution was found by Goldstein and Prandtl (1929) that would achieve the same, but for a propeller. From this, a MIL propeller design procedure was developed by Larrabee (1979, 1983), which determines the chord and twist distributions of a propeller (depending on flow properties and some user-defined propeller properties).

If the incoming flow is parallel to the propeller rotation axis (axisymmetric), its loading is independent of the azimuthal angle. However, if the freestream velocity vector is slightly angled with respect to the propeller axis, the propeller will produce oscillatory loads. As one of the blades now travels more in the direction of the freestream velocity its effective incoming velocity will be slightly lower compared to the other one traveling "against" the freestream flow. This results in the former producing less lift and the latter blade producing more lift and drag than the blades in the vertical orientation. This also produces pitching and yawing moments (due to one side of the propeller producing more thrust than the other) and a normal force, which directly contributes to the total lift of the aircraft. Such situation could arise simply because the wing induces some upwash in front of it where the propeller is usually mounted. Numerous analytical (e.g. by De Young (1965) or Leng et al. (2019)) and experimental (e.g. by Ribner (1945)) studies were done on this topic. When the propeller is not axially aligned with the freestream flow the slipstream will also be somewhat deflected, because both the freestream and the induced axial flow of the propeller will try to force it in their own direction so an equilibrium establishes somewhere in between. If the thrust coefficient of the propeller is high, the slipstream will tend to align more with the propeller axis, however if it is small, the freestream velocity will dictate the inclination (De Young, 1965).

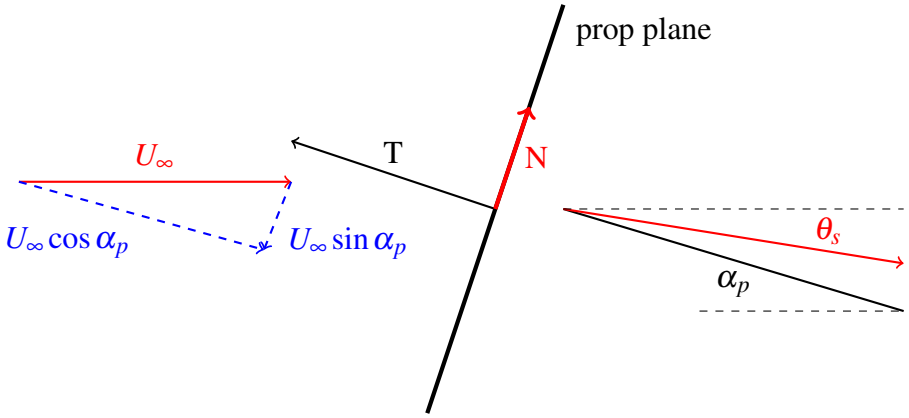

Figure 2.2: Schematic representation of slipstream deflection.

Propeller naturally induces axial and rotational momentum on the freestream flow. Most of it is concentrated in the area behind it called the slipstream. Due to the bound circulation the blades shed vortices, the largest being at the tip due to the large discontinuity in the loading. They travel along the slipstream in a form of a helical vortex sheet. The helix angle is a ratio of the tangential (swirl) velocity and axial velocity. The former is usually assumed to be induced in its totality at the rotor plane and to be constant throughout the slipstream (in inviscid flow), while the latter gradually increases ahead and behind the rotor plane. In the far-field the induced axial velocity is twice the magnitude as at the rotor. As the axial velocity of the slipstream increases, its cross-sectional area will tend to decrease to conform to the mass conservation law. The acceleration of the slipstream (and thus contraction) is largely dependent on the loading of the rotor (thrust coefficient) and for lightly loaded propeller discs it will only amount to a couple of percent of contraction, while for heavily loaded rotors it can rise to around 25% (Conway, 1998).

The simplest model for analyzing a rotor is the Actuator Disk Theory. It is an application of the Momentum Theory, based on the conservation of mass and momentum, where a propeller is modelled as a thin disk which presents a discontinuity in an incompressible and inviscid flow field. The disk presents no resistance to the fluid but it imparts a uniformly arranged force on it in a form of a discontinuous pressure jump. It imparts no rotational velocity to the flow. It is useful for preliminary designs as it is very computationally efficient, however it fails to predict many effects, that are present in real propellers, like the tip vortices, wake swirl, ununiform load distributions, propeller efficiency or blade loading distributions. It does not give a clear relationship between propeller geometry and the produced forces, however it can be useful to analyze the flow field around the propeller and the slipstream. It is mostly used in CFD simulations as a crude representation of a propeller, however in order to also predict the swirl velocities either the rotating actuator disk (Wu and Porté-Agel, 2011) or the actuator line model (Sørensen and Shen, 2002) can be used. An improvement on the former called the regionalized actuator disk was presented by Wang et al. (2014), which divides it into several regions for which the pressure jumps and tangential velocity parameters are obtained with an optimization method in order to more accurately capture their spanwise and circumferential distribution.

By combining the Momentum Theory with the Blade Element Theory, which assumes that the performance of a blade can be represented by a sum of forces acting independently on a number of 2D spanwise sections, the Blade Element Momentum Theory is formed. It is a more

accurate model than the Actuator Disk Theory, as it takes into account the propeller geometry and the radial distribution of the inflow and induced velocities. It is also more computationally expensive, however it is still much faster than a full CFD simulation. Usually it takes in the lift and drag coefficient curves of the blade sections and the geometry of the propeller as inputs. Because this theory is inherently pretty simple some corrections can be applied in order to increase its accuracy. The most common and effective is the Prandtl tip loss correction (Prandtl, 1923) which accounts for the losses due to the generation of the tip vortex. Analogously, BEMT predicts too high lift at the hub so a similar correction can be applied at the root of the blade. Furthermore, BEMT fails to predict cases with very high loading so the Glauert correction (Glauert, 1983) can be applied to compensate for it. Another useful correction is the post-stall correction, which is used to adjust the lift and drag curves of the blade sections after they have stalled. The most common one is the empirical correction by Viterna and Corrigan (1982).

The last propeller evaluation method that will be mentioned is the full-propeller modelling using either lifting lines or vortex lattices to repesent the propeller blades. Here the trailing and shed vortices in the wake actually have to be calculated and their induction at the control points on the blade represented using the Biot-Savart law. The first way this can be done is by using the steady method where the wake is assumed to be a fixed helical structure whose geometry is defined by the propeller geometry and the axial and rotational velocities. The strength of the wake vortices is calculated iteratively through the bound circulation gradient. The second way (the unsteady method) is to calculate the convection and evolution of the wake as it moves downstream. This is useful if the goal is to analyze how the propeller behaves in transient conditions. The wake can either be free, which means that it is free to deform under the influence of other vortex filament, or it can be frozen, which means that its geometry is defined only by the unperturbed flow and only the vortex filament strengths are calculated.

2.3 Effect of the Propeller and its Slipstream on the Wing

The additional velocities in the slipstream certainly have an effect on the wing's inflow conditions and consequentially performance. The most influential are definitely the increase in axial velocity (and thus dynamic pressure) and the introduction of swirl. Furthermore, there can appear some additional induced angles due to the contraction of the slipstream and the inclination angle of the slipstream, and lastly, the chaotic and energetic flow in the slipstream can have a positive effect by re-energizing the boundary layer and help it stay attached to the wing surface at higher angles of attack.

2.3.1 Slipstream Models

The most used model for predicting the velocities induced by an actuator disk and its slipstream is the slipstream tube model which arises from the vortex theory presented by Glauert (1983). It presents the entire vortex field with four different vorticity distributions, namely the ring vortices on the outer surface of the slipstream, the hub vortex along the axis of symmetry, the radial vortex distribution on the actuator disk surface and the longitudinal vortex system on the surface of the slipstream. Their superposition creates the helical vortex structure that is expected from a propeller slipstream vortex system and by using the Biot-Savart law the induced velocity field of the entire slipstream can be calculated.

Many different papers presented the procedure for calculating the development of the axial velocity profile (Metcalfe (1985), Miranda and Brennan (1986)), however the one that appears most in recent papers is the procedure by Conway (1995). He presents the formulas for a general, polynomial and elliptic blade loading distributions, the latter being the simplest, however if the assumption of having an elliptic loading distribution is too extreme, the formulation for a general loading can be utilized. These procedures allow for the calculation of induced velocities even outside of the slipstream boundaries and in front of the propeller plane, however they also assume a constant tangential velocity throughout the slipstream.

If a lifting line or a vortex lattice is used to represent a propeller blade in an unsteady simulation, the development of the wake can be directly calculated by figuring out the velocity of different vortex points shed from the propeller blades. At each time step a vortex is shed at every spanwise blade location with the strength equal to the spanwise change in circulation. Its velocity is dependent on the free stream velocity and the induced velocities from every other bound or trailing vortex in the system. For this reason the complexity of this problem increases exponentially with time. As discussed before, either a free or a frozen wake can be utilized, depending on the wanted accuracy of the model.

2.3.2 Effects of Increased Axial and Tangential Velocity

The main influence of increased axial velocity in the slipstream of the propeller is the increase in dynamic pressure, which is directly linked to the local generated lift and drag. As the slipstream axis is more or less aligned with the freestream flow this simply results in a higher local inflow velocity, which is now a function of the spanwise position. The local increase of the inflow velocity, however, also influences some geometric angles like the wing induced angle of attack because it is a ratio of downwash and the local free stream velocity. If the propeller is inclined with respect to the freestream (i_p), lets say tilted down, the induced axial velocities at its location will point slightly up, which will increase the local effective angle of attack of the wing (ϕ).

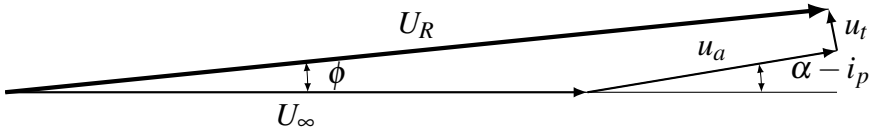

Figure 2.3: Vector diagram behind the up-going blade side of the propeller.

The tangential induced velocities are usually smaller in magnitude compared to the axial induced velocities, however they play a crucial role in determining the effective local angle of attack of the wing. Since behind the up-going blade side the slipstream rotates up, this adds a vertical component to the resulting inflow velocity, effectively increasing the local angle of attack (this situation is represented in figure 2.3). The opposite holds for the down-going blade side of the propeller (u_t would point down, decreasing ϕ). The bigger the ratio between the tangential induced velocities and the combined axial velocities the larger the increase in local angle of attack. This effect, called the stator vane effect, effectively reduces the rotational energy inside the slipstream and utilizes the tangential velocities to reduce induced drag. In

extreme cases where the propeller-induced upwash is higher than the wing-induced downwash, the local lift vector would actually point slightly forward, producing effective thrust.

However the increase in angle of attack on one side of the propeller and decrease on another do not cancel each other out. By combining them with the increase in loading due to the increased dynamic pressure on both sides of the propeller, the effect behind the up-going blade side of the propeller benefits double-fold, while on the other side of the propeller the loading is usually slightly reduced compared to the propeller-off condition. Nevertheless, the net result is usually favorable. In general propellers that are rotating inboard-up increase lift more and induce less drag than propellers rotating outboard-up due to the more favorable superposition of induced velocities (Veldhuis, 2005).

2.3.3 Effect of Slipstream Contraction

As the slipstream contracts behind the propeller plane it induces some upflow at its bottom side and some downflow at its top side (see figure 2.4). Depending on the vertical location of the wing inside the slipstream this effect can result in some additional induced inflow angle to the wing. This was observed by Veldhuis (2005) and Fei et al. (2018), who also presented a linear relationship between the lift coefficient of an unblown wing and the vertical position of the propeller to achieve maximum lift. The contraction (and therefore the flow angle) is highest immediately after the rotor plane at the edge of the slipstream. Yet a very high or low vertical position of the propeller with respect to the wing would also result in a much lower area of the wing being submerged in the slipstream, greatly reducing the effects of the increased axial and tangential velocities. Analogously the contraction also induces some spanwise flow in the horizontal plane, however this does not have a big effect on the final wing loading.

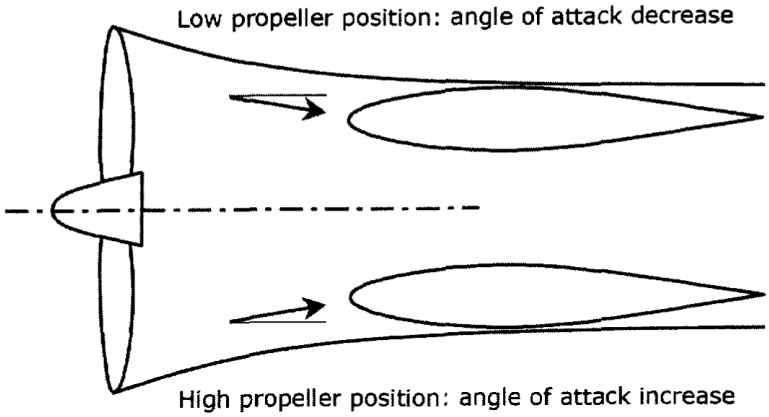

Figure 2.4: Representation of the slipstream contraction effect. Image taken from Veldhuis (2005).

2.3.4 Effect of Slipstream on the Wing's Boundary Layer

Without the presence of a propeller the flow in the boundary layer on the top surface of the wing usually starts as laminar, with a possible laminar separation bubble present, and at some point along the chord it transitions to turbulent flow. By increasing the angle of attack the transition point tends to migrate towards the leading edge of the wing and at some point separation might occur, causing a rapid drop in lift and increase in drag. By introducing a propeller slipstream,

several interesting phenomena occur. Inside the slipstream the flow over the wing transitions from laminar to turbulent quite early on and it stays that way up to the trailing edge. There is also no laminar separation bubble. Furthermore, Aminaei et al. (2019) and Veldhuis (2005) both observed, that the presence of a slipstream also had an effect outside the slipstream. Due to the mixing with the surrounding flow the transition from laminar to turbulent flow occurs earlier. Because of this, separation is often delayed, Aminaei et al. even found out that at higher angles of attack, the flow did not separate at all close to the propeller centerline. In the large turbulent region inside the slipstream the skin friction naturally increased due to high wall shear stresses.

2.4 Effect of the Wing on the Propeller and the Slipstream

Veldhuis (2005), Alba et al. (2018) and Cole et al. (2013) all observed that when modelling propeller-wing interaction it is of vital importance that the effects of the wing on the propeller and its slipstream is also taken into account. The latter specifically calculated that there is a 12.5% discrepancy in span efficiency whether single-sided interaction of full-interaction model was used. Without considering the effects of the wing, the effects of the propeller would tend to be overpredicted, resulting in the final predicted lift of the wing being too high.

2.4.1 Effect of Wing Upwash

The bound circulation of the wing produces upwash in front of it, causing the inflow angle to the propeller to change. This effects not only the propeller which is now likely under the influence of non-axial inflow conditions, but also the slipstream which gets deflected even more along its path from the propeller to the wing. Because of the non-axial inflow conditions the load of the blades now varies with the azimuthal angle, producing an oscillatory load, increasing vibrations and fatigue on the blades. Moreover, a normal force is produced which directly contributes to the effective lift of the propeller-wing assembly, alongside pitching and yawing moments. Heidelberg and Woodward (1987) discovered that the inflow angle to the propeller changes with the rate of 1.5 compared with the angle of attack of the wing for their particular setup and that it is nearly constantly distributed along the span of the wing.

2.4.2 Swirl Recovery

The next important effect of the wing on the slipstream is the swirl recovery effect. The wing acts as a stator vane which reduces the swirl, namely decreasing the tangential velocities. This effect is tightly connected to the increase in local angle of attack by the rotation of the slipstream wherein the "positive" effect on the wing will result in a "negative" effect on the slipstream. The simplest way to model this is to use a swirl recovery factor (SRF) introduced by Veldhuis (2005). In his work he used a constant value of 0.5 which results in a reduction of tangential velocity magnitude by half. Alba et al. (2018) observed that this value is usually to low and developed an active routine that calculates the rotational kinetic energy at several stations along the sliptube and how it reduces due to the presence of the wing. This way they were able to take into account different wing geometries and operating conditions and more accurately obtain the SRF which would, depending on the inner and outer wing twist, range from 0.3 all the way up to 1.0.

2.5 Lift-Augmenting Propellers

Distributed propulsion systems use multiple propellers with the goal to spread out the production of induced velocities along the entire wing and augment its lift more compared to a single propeller. With this in mind it makes sense to look for propeller designs that augment the lift of the wing behind them more than a propeller designed for maximum efficiency. Chow et al. (1970) studied the effects of different velocity profiles of non-uniform streams on the lift generated by an airfoil submerged in it. They used three parameters to describe a velocity profile: a is the maximal induced velocity factor and represents the maximal velocity of the velocity profile, d is the characteristic width of the velocity profile and z_s is the vertical distance of the airfoil from the velocity profile centerline.

Through numerical simulations of airfoils submerged in different velocity profiles shapes described by a non-uniformity parameter a/d^2 they observed a general trend of the airfoil producing higher lift coefficients when the non-uniformity parameter was lower, i.e. a was small or d was big, pointing towards a more uniform stream. Patterson (2016) showed with numerical simulations that such propellers, designed with a goal of producing a uniform axial velocity profile, tend to consume less power and produce less thrust for the same average induced axial velocity generated. The reason why requiring less power is obvious, however having the propellers produce less thrust is especially useful during landing phase of flight when we want the most amount of lift at the lowest velocity possible.

Figure 2.5 shows this effect for optimal z_s values where C_L is highest. It can clearly be seen how the C_L is increased as the velocity profile gets more uniform.

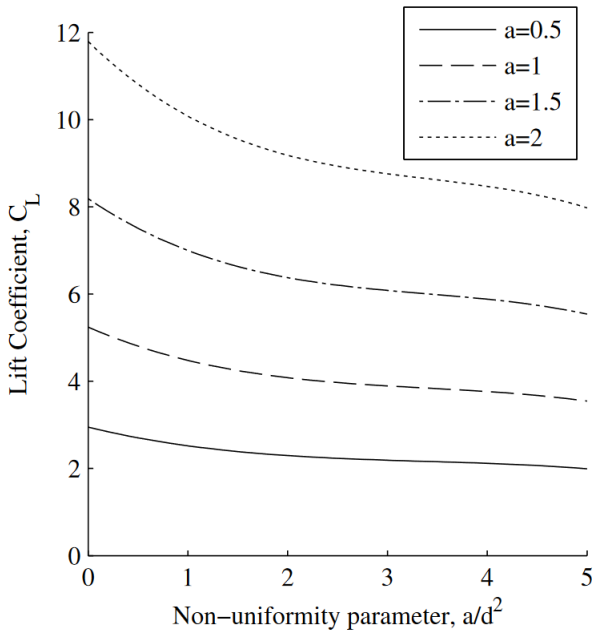

Figure 2.5: Wind lift coefficient as a function of the non-uniformity parameter a/d^2. Image taken from Patterson (2016).

Another important observations that can be made from figure 2.5 is that the effect of non-uniformity is higher at higher induced velocities, meaning that the shape of the slipstream

velocity profile will have a greater effect at higher thrust coefficients.

These observations are important because the main objective of a lift-augmenting (LA) propeller is to increase the lift of the wing behind it as much as possible and if we can design a propeller in such a way so that the velocity profile in its slipstream is as uniform as possible this will, at least in theory, increase the lift of the wing more.

2.6 Optimization Algorithms

Optimization algorithms are a mathematical methods for (usually) minimizing one or more objective functions in order to find the solution that is as close as possible to the optimum. They adjust the optimization parameters and learn from previous generations/iterations to hopefully find a sufficiently good combination of parameters. Multi-objective (MO) optimization algorithms differ from single-objective (SO) algorithms in that the solutions must conform to two or more, usually contradicting, objective functions (e.g. maximizing lift and minimizing drag). SO optimization algorithms will return the sole best solution, while MO optimization algorithms will return a series of solutions on the so-called Pareto front which consists of non-dominated solutions that are a compromise between the multiple objectives. Following is a description of two multi-objective metaheuristic optimization algorithms that are inspired from different processes in nature in order to strive towards the best solution and will be used later as methods to find the design trends of different DEP configurations for most efficient flight.

2.6.1 NSGA-II

Genetic algorithms are a branch of evolutionary algorithms that model natural processes like natural selection, crossover and mutation to find the fittest specimen or solution. An optimization variable can be thought of as a gene, a combination of genes (a chromosome) represents a solution that is being evaluated and set of chromosomes is a population of a certain generation. The goal of the algorithm is to evaluate the the solutions according to some objective function and select the best from the current generation, mutate them and create a new population for the next generation. This process is repeated N times of until a certain convergence is achieved. In the end a genetic algorithm returns one or multiple solutions and their variables that are better than the rest with respect to the objective function.

One of the most popular multi-objective genetic optimization algorithms is NSGA-II, developed by Deb et al. (2002). It builds on NSGA, mainly reducing computational cost from $O(MN^3)$ to $O(MN^2)$ (where M is the number of objectives and N is the population size), including elitism and including the specification of the sharing parameter to ensure diversity. It's key features are fast non-dominated sorting, that classifies solutions into fronts by domination, crowding distance, which ensures that the solutions are spread apart in order to promote exploration, and elitism, which carries over a couple of best solutions to the next generation so they are not lost through mutation.

The optimization process starts by producing a random initial parent population. It is sorted based on non-domination and each solution is assigned a rank. The first iteration is slightly different due to lack of elitism but afterwards the procedure goes as follows: through selection, mutation and recombination an offspring population Q_t with size N is created. It is combined

with the original parent population P_t and sorted by dominance. If there are less than N solutions in the first rank, all of them are included in the new parent population and the subsequent ranks are looked at until N solutions are selected (see figure 2.6).

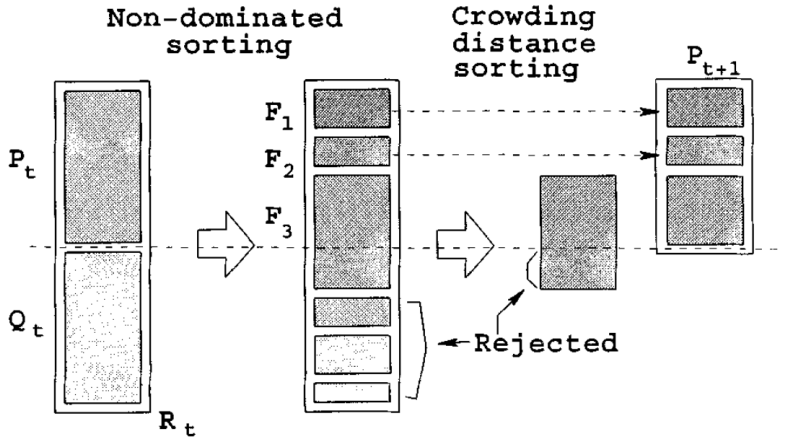

Figure 2.6: NSGA selection procedure. Image taken from Deb et al. (2002).

NSGA-II also includes a constraint handling procedure. In the binary tournament selection where two solutions are compared against each other, there can be three possible situations:

1. If both solutions are feasible the solution with better objective function value is chosen.
2. If one solution is feasible and the other one is not, then the feasible solution is chosen.
3. If both solutions are unfeasible the solution with smaller overall constraint violation is chosen.

NSGA-II also requires crossover and mutation operators as inputs (η_c and η_m). The first controls the spread of the offspring solutions while the second controls the extent of mutation of offspring solutions. Lower values of η_c will result in larger variation of offspring, encouraging exploration, while higher values will result in offspring solutions being closer to the parent solutions, encouraging exploitation. Similarly, lower values of η_m will result in larger mutation of offspring, encouraging exploration, while higher values will result in offspring solutions being closer to the parent solutions, encouraging exploitation. By utilizing larger values, more of the design space is explored, which also reduces the risk of getting stuck in a local minimum and premature convergence. Lower values of η_c and η_m are useful when the design space is well understood and the goal is to refine the solution.

2.6.2 SMPSO

Speed Constrained Multi-objective Particle Swarm Optimization (SMPSO) algorithm, developed by Nebro et al. (2009), is an improved version of OMOPSO (a version of MOPSO, a Multi-Objective Particle Swarm Optimization) which is a type of Particle Swarm Optimization algorithm. Like genetic algorithms, PSOs are inspired by processes in nature, specifically social behavior like the movement of a flock of birds or a school of fish (Kennedy and Eberhart, 1995).

Every solution is represented by a "particle" and a collection of them is called a "swarm". Each particle is characterized by its position and velocity. The latter is adjusted according to the particle's previous velocity, the cognitive component, which forces the particle to move towards its personal best position, and a social component, which tries to move the particle towards the best position of the entire swarm. The optimization terminates when certain convergence is achieved.

3

MIL and LA Propeller Design and Analysis

The first step in building the final optimization procedure was to set up two different propeller design methods: the lift-augmenting (LA) propeller and the minimum induced loss (MIL) propeller. This involved understanding the fundamental propeller analysis theories, which are described in section 3.1 together with the procedures used for designing MIL and LA propellers will be presented. The next section (3.2) focuses on predicting the behavior of the propeller slipstream. Following is a section that evaluates the accuracy of the propeller performance prediction methods used in this work by comparing them to experimental data (3.3). Lastly, in section 3.4, the differences between the MIL and LA propellers are discussed.

3.1 Propeller Analysis and Design

Blade element momentum (BEM) is one of the most used propeller analysis theories used during the initial stages of propeller and aircraft design. It will be utilized throughout this research, both for propeller design and evaluating its off-design performance. Although quite simple, it produces relatively accurate results if certain assumptions are not violated, mainly:

- steady, inviscid and incompressible flow,
- independent blade element sections with 2D flow,
- no radial flow,
- infinite number of blades (if corrections are not applies) and
- no wake expansion.

3.1.1 Momentum Theory

The first part of the BEM is momentum theory, which models steady, incompressible flow of a streamtube that gets accelerated by an actuator disk, which is an infinitely flat disk that uniformly imparts a force on the flow (and vice versa) and creates a discontinuous pressure difference between its front and back sides. Depending on the direction of this force it can

either represent a propeller or a rotor. By imposing steadiness, inviscidness, incompressibility constant internal energy to the continuity, momentum and energy equations the expressions for velocity, thrust and power at the actuator disk can be obtained.

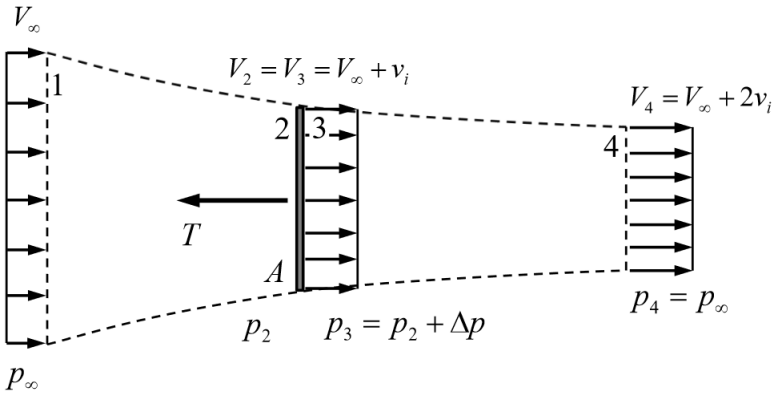

Figure 3.1: Actuator disk acting as a propeller. Image taken from Patterson (2016).

$$V_2 = V_3 = V_R = \frac{1}{2}(V_1 + V_4) \tag{3.1}$$

$$T = \rho V_1^2 A_1 - \rho V_4^2 A_4 = 2\rho(V_1 - V_R)V_R A_R \tag{3.2}$$

$$P_R = TV_R = 2\rho(V_1 - V_R)V_R^2 A_R \tag{3.3}$$

Through the continuity equation the change of velocity along the actuator disk centerline can be obtained. As mass flow is constant (due to the incompressibility assumption) the velocity will change inversely to the cross-sectional area of the streamtube. Likewise, the pressure will follow the Bernoulli's principle in front of and behind the actuator disk while at it's location it will discontinuously increase (if it represents a propeller) or drop (if it represents a turbine). The thrust is equal to the change in pressure over the disk times its area.

By defining a new variable a called the axial induction factor which tells us how the actuator disk changed the freestream velocity, the upper equations can be rewritten into a simpler form.

$$V_R = (1 + a)V_\infty \tag{3.4}$$

where a is the ratio of the axial induced velocity immediately after the rotor and the freestream velocity:

$$a = \frac{v_a}{V_\infty} \tag{3.5}$$

$$\frac{T}{\frac{1}{2}\rho V_\infty^2 A_R} = C_T = 4a(1 + a) \tag{3.6}$$

$$\frac{P}{\frac{1}{2}\rho V_\infty^3 A_R} = C_P = 4a(1+a)^2 \tag{3.7}$$

The the momentum theory is a simple way to analyze 1-dimensional rotor performance under certain assumptions. It must be kept in mind that due to one-dimensionality it can not predict torque and radial distribution of loading.

3.1.2 Blade Element Momentum Theory

The Blade Element Momentum Theory combines the Momentum theory with the Blade Element Theory. It was developed in order to overcome Momentum Theory's downside of not being able to account for rotational velocities and specific blade shapes.

The Blade Element Theory uses strip analysis to divide the actuator disk in the radial direction into infinitesimally small annuli. If the lift and drag curves of the airfoil at each radial station is known the local forces can be calculated which depend on the local velocity W. It consists of rotational (Ωr), freestream (V_∞) and induced velocities (v).

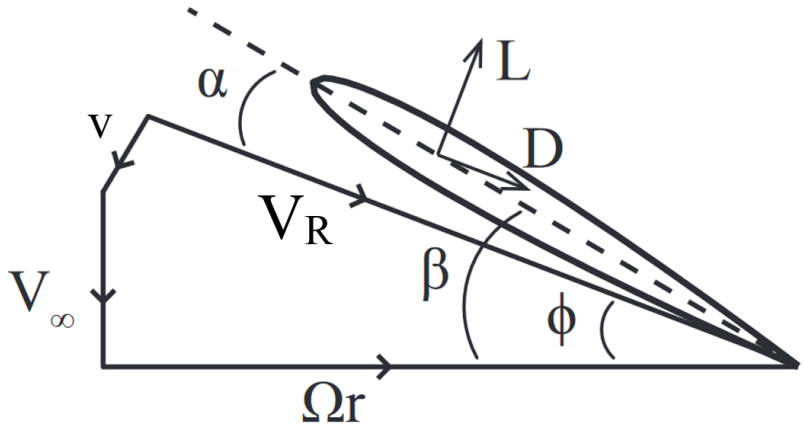

Figure 3.2: 2D blade section geometry definitions. Image taken from Patterson (2016).

The thrust and torque at each annulus can be calculated with the following equations:

$$dT = Bc\frac{1}{2}\rho V_R^2(c_l cos\phi - c_d sin\phi)dr \tag{3.8}$$

$$dQ = Bc\frac{1}{2}\rho V_R^2(c_l sin\phi + c_d cos\phi)rdr \tag{3.9}$$

Through integration the thrust and torque produced by the entire rotor can be obtained.

Similarly to how the axial induction factor a was defined in section 3.1.1 the tangential induction factor can be defined by looking at how the local angular velocity directly aft of the propeller (ω) changes compared to the rotational rate of the propeller.

$$a' = \frac{\omega}{2\Omega} \tag{3.10}$$

By utilizing the previously defined axial induction factor a and the newly defined tangential induction factor a' momentum theory-based counterparts of equations 3.8 and 3.9 can be obtained:

$$dT = 4\pi r \rho V_\infty^2 (1+a) a dr \tag{3.11}$$

$$dQ = 4\pi r^3 \rho V_\infty \Omega (1+a) a' dr \tag{3.12}$$

By equating equation 3.8 with 3.11 and equation 3.9 with 3.12 the induced velocity factors can be calculated with the use of an iterative scheme. Furthermore, in subsequent sections these equations will be used to calculate the chord distribution of the blade from the induced factor distribution.

To reiterate, BEMT in its most common form is only possible due to a couple of assumptions. One of them, that has a lot of influence on the final result and makes it quite inaccurate, is the assumption that the blades behave like they are infinitely long, specifically that they do not produce a tip vortex. In reality, the tip of the blade sheds a vortex that significantly reduces the loading as we move towards it. This happens due to the tip vortex inducing a certain negative angle of attack and thus reducing the effective local angle of attack. All of this can however be corrected for via the Prandtl tip loss factor which gets applied to the axial induction factor ($a_{corr} = \frac{a}{F}$).

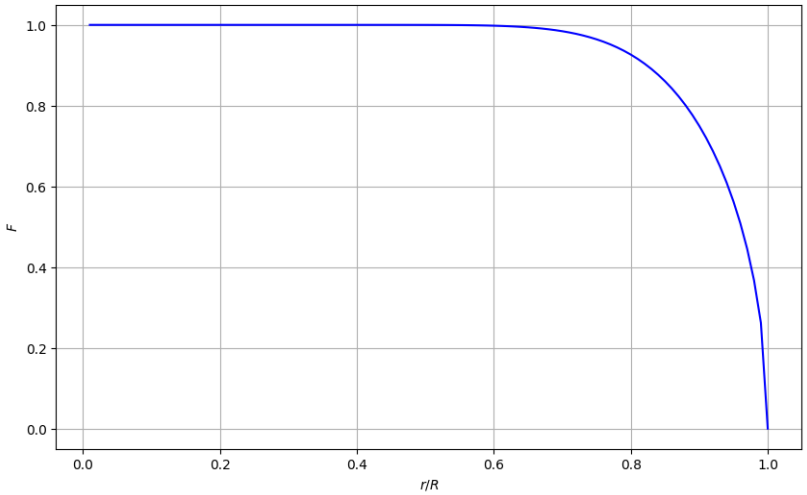

Figure 3.3: Prandtl tip loss factor distribution along the blade.

$$F = \frac{2}{\pi} \cos^{-1}(e^{-f}) \tag{3.13}$$

$$f = \frac{B}{2}\frac{1-r}{r\sin(\phi)} \tag{3.14}$$

where the inflow angle ϕ is defined as

$$\phi = \frac{V_\infty(1+a)}{\Omega r(1-a')} \tag{3.15}$$

3.1.3 Designing the Propellers

Two propeller design techniques were used throughout this thesis. The first one is one of the most common propeller design methods, the minimum induced loss (MIL) propeller design method. The second one is the lift-augmenting (LA) propeller design method.

Minimum Induced Loss Propeller Design

In the DEP configuration that is being researched in this thesis the MIL propellers will be used both during take-off and cruise, providing all thrust during the latter. They were designed following Larrabee's procedure for designing MIL propellers (1979, 1983). It is fairly straightforward and allows us to also obtain the induced velocity factors needed for slipstream development calculation, propeller thrust coefficient and efficiency. It also allows the designer to either specify needed propeller thrust or power. Other parameters that need to be determined beforehand are some flow conditions (freestream velocity and density), propeller number of blades, tip radius, hub radius, RPM and airfoil polars (for lift and drag coefficients).

Lift-Augmenting Propeller Design

Up until now, a lot of research done on the aircraft propellers was done to increase their efficiency of producing thrust throughout the entire operating envelope of the aircraft. However, lift-augmenting propellers have to be designed with a different mindset. In fact, during landing, their aim should be to increase the lift of the wing as much as possible by producing as little extra thrust as possible, because the aircraft needs to be slowed down. The aim of this section is to find a way to design a propeller, that will increase the lift of the wing behind it the most.

As discussed in section 2.5, according to theory, the biggest lift augmentation of a wing with a propeller in front of it is observed when the velocity profile in the slipstream is as uniform as possible. Naturally, if the propeller also produces higher average axial velocity in the slipstream with an equal amount of power it also augments the lift more. Hence, the starting point of designing such propeller will be to have a constant distribution of a to which some tip and root corrections will be applied in order to make it more physically correct and ensure that the final propeller geometry is manufacturable. The propeller hub and tip radii, propeller RPM and power, free-stream velocity and density should be determined by the user. The polars, needed to obtain c_l and c_d values, can be generated with XFOIL (Drela, 1989).

The iterative procedure used to calculate the induction factors distributions along the propeller blades is described by Patterson (2016). He included two additional steps, the first being the use of the Prandtl tip loss factor which requires the use of an iterative scheme, and the second

one being the restriction of a' spanwise gradient, because rapid changes of tangential induction factors in the spanwise direction result in rapid changes in chord and twist distributions. Consequently, the final propeller design might be aerodynamically efficient but impossible to manufacture.

3.2 Propeller Slipstream

Now that the geometry and the induction factors of the propeller are defined the velocities and other properties of its the slipstream can be calculated. Drela (2006) presented a way of calculating the tangential velocity distribution immediately after the propeller plane based on the blade circulation distribution.

$$v_t(r,0) = \frac{B\Gamma}{4\pi r} \frac{1}{F\sqrt{1+\left(\frac{4\tan\phi}{\pi B}\right)^2}} \cdot SRF \tag{3.16}$$

This distribution will be assumed constant throughout the slipstream or at least up to the wing's quarter chord position (Conway, 1995). From geometry, as described by Chandrasekaran (1986), an expression for v_a based on v_t can be obtained:

$$v_a(r,0) = 0.5\left[-V_\infty \cos\alpha + \sqrt{(V_\infty \cos\alpha)^2 + 4v_t(\omega r - v_t)}\right] \tag{3.17}$$

The change in axial velocity profile downstream of the propeller will change more significantly than the tangential velocity profile, moreover, it has a bigger effect on the final loading of the wing. Therefore it is important that the axial development of the induced axial velocity profile is taken into account. As was observed in the chapter about momentum theory, the average axial velocity in the slipstream is constantly increasing, but the rate of change of this increase is highest immediately after the propeller. This means, that if the propellers that are closer to the wing, he latter will experience lower velocity flow than if they were mounter further away. Moreover, since one of the main assumptions of this work is based on the uniformity of axial velocity profile behind the propeller for greater lift augmentation it is important to also observe how it changes along the slipstream. Conway (1995) presented a method for capturing the flow development inside of a slipstream for arbitrary loading, alongside a simplified version for an even polynomial, parabolic and an elliptic radial loading distribution. The latter is most commonly used in many other papers (Alba et al., 2018 and Epema, 2017) due to its simplicity, however elliptic distribution is not very uniform. For this reason it was decided to use the slightly more complex arbitrary radial loading development calculation.

$$v_a(r,x) = 2v_a(r,0) - \int_0^R \int_0^\infty v_a(r',0)e^{-s|x|}sr'J_0(sr')J_0(sr)dsdr' \tag{3.18}$$

The upper equation gives us the axial velocity at any radial station along the slipstream. J_0 is the Bessel function of the first kind with $n = 0$. In order to obtain the full profile this function has to be applied to all r in the radial direction. This procedure is therefore relatively computationally expensive, however the obtained profile is definitely closer to the one produced by the designed

propeller in reality than if just an elliptic profile distribution would have been taken, which would produce a similar axial velocity profile for both LA and MIL propellers, which defeats the purpose of designing two different propellers.

To approximate the contraction of the slipstream the following formula developed by Veldhuis (2005) according to Theodorsen's theory can be used.

$$\frac{R_S(x)}{R} = \sqrt{\frac{1+a}{1+a\left(1+\frac{x}{\sqrt{R^2+x^2}}\right)}} \tag{3.19}$$

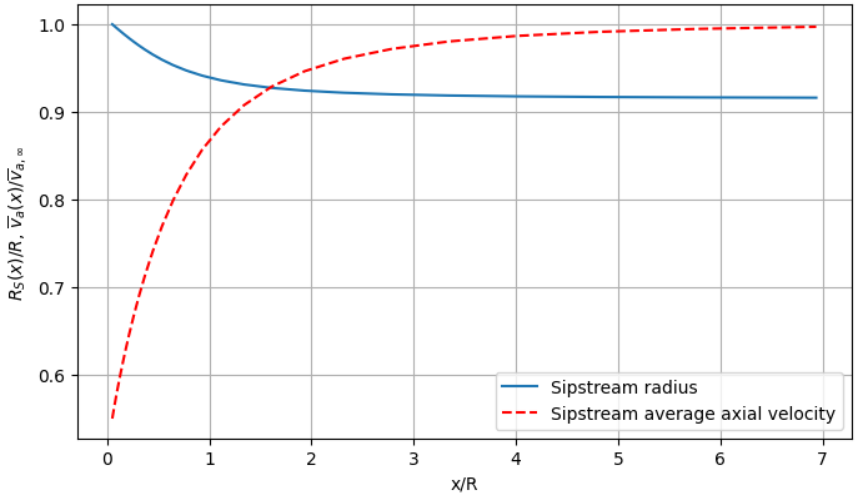

Figure 3.4: Axial development of slipstream radius and average axial velocity; $C_T = 0.298$.

Here, a is the already known axial velocity induction factor, dependent on the thrust coefficient C_T and x is the station along the slipstream at which we want to know its radius. It can be inferred that by producing a higher thrust coefficient, the slipstream will contract more and thus decreasing the washed are of the wing, however the induced flow angle due to contraction will also increase. The axial development of the slipstream radius and average axial velocity can be seen in figure 3.4. It can be observed how the average axial velocity far downstream of the propeller plane is twice the average axial velocity at the propeller plane, as it should be according to the momentum theory. The propeller slipstream contracts less than 10% in the presented case and most of the contraction happened before $x/R = 3$.

Simulating propeller performance with actual non-axisymmetric inflow conditions is difficult. Therefore, some models were developed to approximate the normal force and the slipstream deflection of a propeller whose performance is obtained for axisymmetric conditions. In order to calculate the normal force coefficient due to the inclination of the propeller against the free stream and the deflection angle of the slipstream (assumed constant), the de Young's procedure can be utilized.

$$\frac{dC_N}{d\alpha_p} = \frac{4.25\sigma_e}{1+2\sigma_e} \cdot \sin(\beta_0 + 8) \cdot f \cdot \frac{\pi J^2}{8} \tag{3.20}$$

$$\sigma_e = \frac{4B}{3\pi} \cdot \frac{c_{av}}{2R} \cdot \frac{C_{l_{av}}}{0.95 \cdot 2\pi} \tag{3.21}$$

$$f = 1 + 0.5 \cdot \left[\sqrt{1+T_C} - 1\right] + \frac{T_C}{4(2+T_C)} \tag{3.22}$$

$$T_C = \frac{8}{\pi J^2} \cdot \frac{T}{\rho n^2 D^4} \tag{3.23}$$

$$\frac{d\theta_S}{d\alpha_p} = \frac{1+T_C-\sqrt{1+T_C}}{2+T_C} + \frac{3+2T_C+\sqrt{1+T_C}}{2+T_C}^2 \cdot \frac{\sqrt{1+T_C}}{4} \left.\frac{dC_N}{d\alpha_p}\right|_{T_C=0} \cdot \frac{8}{\pi J^2} \tag{3.24}$$

Equation 3.20 results in the gradient of the normal force coefficient with respect to the inclination of the propeller rotation axis to the inflow velocity vector. σ_e represents the effective solidity of the propeller, c_{av} is the average blade chord and $C_{l_{av}}$ is the average lift curve slope of the individual blade polars. f is the thrust factor and is a function of the freestream dynamic pressure based thrust coefficient T_C, while β_0 is the blade pitch angle (with respect to the zero-lift line) at the 0.75 blade span location. Though the normal force of the propeller contributes to the total lift of the wing its effect is usually rather small due to the small inflow angles (the vertical component of propeller thrust is usually larger). However, the normal force slope is needed to calculate the propeller slipstream deflection slope $\frac{d\theta_S}{d\alpha_p}$, specifically its value when $T_C = 0$ (equation 3.24). This value will play a big role in the next parts since it greatly influences how the slipstream crosses the wing.

Lastly, the influence on the local angle of attack due to the contraction of the slipstream was incorporated. On the edge of the slipstream the contraction component of velocity will be parallel to the contraction slope, while elsewhere it will be proportional to the radial position inside the slipstream.

$$\delta_{contr}(x, r_S) = \arctan\left(\frac{dR_S}{dx}(x)\right) \cdot \frac{r_S(x)}{R_S(x)} \tag{3.25}$$

3.3 Validation of Propeller Performance

In order to assess whether the results of individual components of DEP configuration analysis and the optimization accurately represent the physical phenomena they need to be validated against experiments or other numerical simulations. The TU Delft's PROWIM propeller was chosen as the reference, because its geometry and performance curves are publicly available and because it will later be used in the propeller-wing interaction analysis. The propeller is a MIL-type 4-bladed propeller with a diameter of 0.236 m. Its geometry was obtained from Niro et al. (2024).

For comparison, in some of the validation cases the same setup was also recreated in DUST - a mid-fidelity open-source aerodynamic solver targeted at unconventional aircraft configurations. It was a product of collaboration between Airbus' A^3 startup accelerator and the Department of

Aerospace Science and Technology of Politecnico di Milano. It is able to run either lifting line, vortex lattice or surface panel elements. One of the most interesting features is the NLVL (non-linear vortex lattice) solver, which combines the benefits of the lifting line and vortex lattice solvers in that it allows a good surface discretization of a vortex lattice while implementing the use of aerodynamic databases to include the viscous correction, like with a lifting line (Savino et al., 2024).

The experimental data for the isolated performance of the PROWIM propeller was taken from Sinnige (2018). The goal of this validation was mainly to analyze how well different numerical analysis methods predicted the performance of a propeller so that any potential offset may be taken into account during optimization. The results produced with DUST were obtained using a linear vortex lattice to model the propeller without any polars since the .c81 files at required Mach and Reynolds numbers and larger angles of attack used by DUST were not easily accessible.

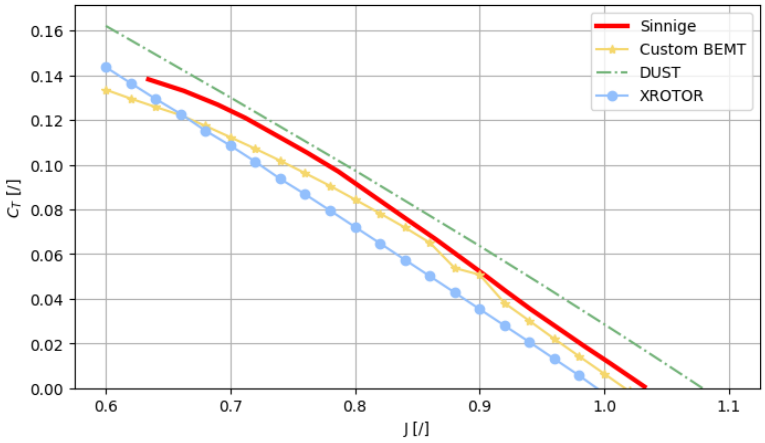

(a) PROWIM thrust coefficient vs. advance ratio.

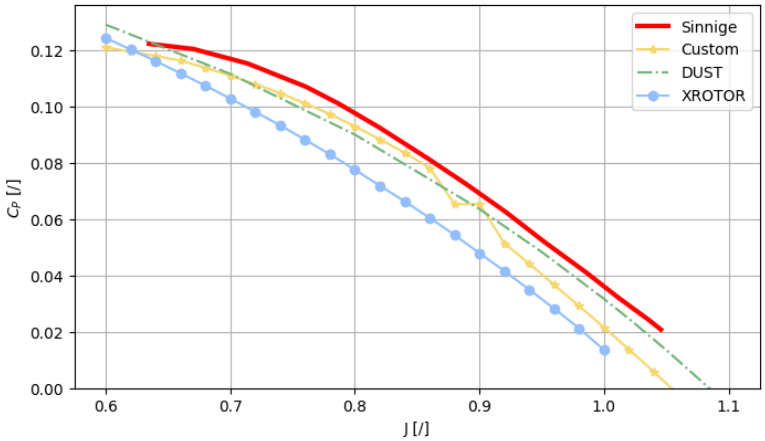

(b) PROWIM power coefficient vs. advance ratio.

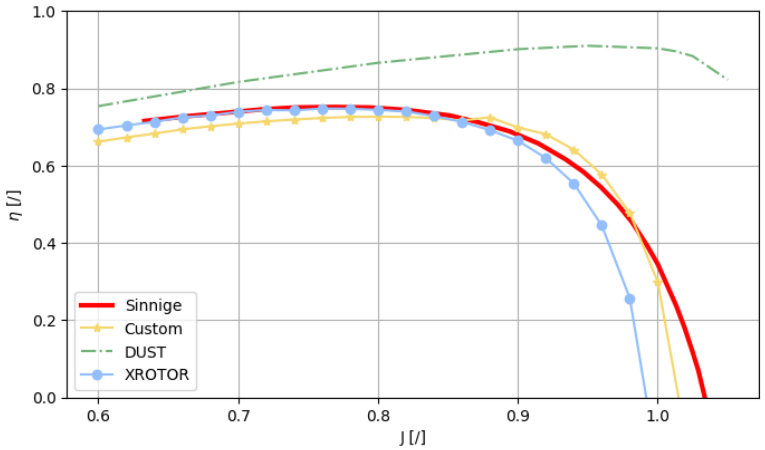

(c) PROWIM propulsive efficiency vs. advance ratio.

Figure 3.5: PROWIM propeller performance validation.

From the upper figures it can be seen how different numerical propeller performance prediction methods compare to the experimental data. All of them manage to predict C_T and C_P quite well, XROTOR being the furthest off. This is likely due to it using a constant lift slope and a

simple parabolic function for drag coefficient prediction. However the main difference can be observed when looking at figure 3.5c, which depends on the ratio between C_T and C_P. Here the custom blade element momentum theory solver fares best, while the prediction of DUST is completely off at higher advance ratios due to the lack of any airfoil polar information and a fixed prescribed lift slope of 2π. It is also interesting to note how both C_T and C_P can appear to be predicted fairly accurately but because the values in question are fairly small their ratio (propulsive efficiency) can be off by a large margin.

3.4 MIL vs. LA propellers

One of the main assumptions regarding the present work is that lift-augmenting propellers, designed according to Pattersons method, are able to produce higher a more uniform axial slipstream velocity profile with higher average axial velocity (at same propulsive power). According to Chow et al. (1970), both of these factors contribute to higher lift augmentation. In this chapter two propellers will be designed, one following Larrabee's minimum induced loss procedure and one following Patterson's uniform slipstream procedure, and their performance will be compared.

As discussed in chapter 3.1.3 the starting point for designing a minimum loss propeller is to find the blade circulation distribution that produces minimal induced loss, similarly to finding the geometry of a wing that produces an elliptical lift distribution. In contrast, the design of a lift-augmenting propeller starts with finding a constant axial induced velocity factor that would satisfied the given power input. Because of these two completely different approaches it is expected that the two propellers will have different performance characteristics.

Due to these two different approaches to propeller design, the axial and tangential induced velocity factor distributions are expected to be different. The axial induced velocity factor distribution is expected to be more uniform for the LA propeller, except towards the root and the tip of the blade due to the utilization of the two correction steps, namely the restriction of the tangential velocity factor gradient at the root of the blade to prevent unfeasible geometry and the inclusion of the tip losses by increasing the axial velocity induction factor proportional to the Prandtl's tip loss factor. Comparison of the axial and tangential induced velocity factor distributions for the MIL and LA propellers can be seen in figure 3.6. The tangential induced velocity factor distribution is slightly higher for the LA propeller at the root of the blade and at the tip due to the need for uniform axial velocity distribution.

Because of these specific increases in axial and tangential induced velocity factors, the chord and twist distributions are also expected to be different. Because a "typical" blade load distribution peaks at around $0.75R$ station the chord has to be much higher at the root of the blade to increase loading in this region. Compared to the one of a MIL propeller, the chord distribution of an LA propeller increases quicker at the start of the blade and shortly afterwards peaks. Then it drops to a steady level which starts to drop off only very close to the blade tip. This happens in order to counteract the tip losses. The twist distributions for the two propellers are fairly similar, however there is a small increase in twist at the tip of a LA propeller, again to counteract the tip losses. Comparison of the normalized chord and twist distributions for the MIL and LA propellers can be seen in figure 3.7.

In order to verify if the generated LA propeller geometry actually produces a more uniform

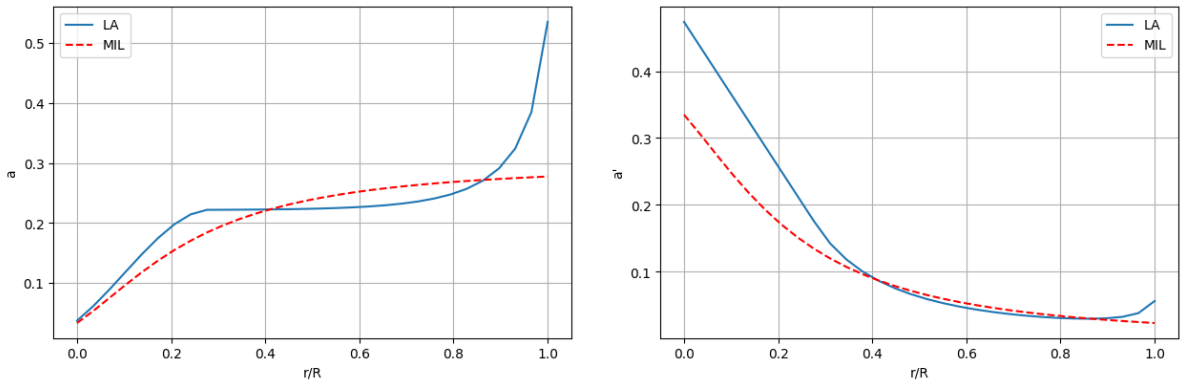

(a) Axial induced velocity factor distribution.

(b) Tangential induced velocity factor distribution.

Figure 3.6: Comparison of axial and tangential induced velocity factor distributions for MIL and LA propellers; $J = 0.8$ and $C_P = 0.294$.

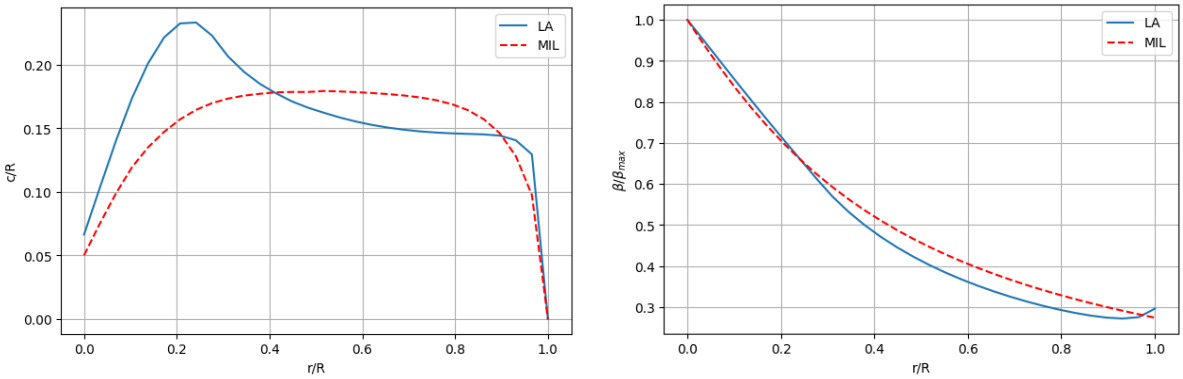

(a) Normalized chord distribution.

(b) Normalized twist distribution.

Figure 3.7: Comparison of normalized chord and twist distributions for MIL and LA propellers; $J = 0.8$ and $C_P = 0.294$.

axial slipstream velocity profile, the axial velocity profiles at different stations downstream were compared. Comparison of the slipstream axial velocity profiles for the MIL and LA propellers at different stations downstream can be seen in figure 3.9. The slipstream axial velocity profile for the LA propeller is in fact more uniform than the one for the MIL propeller. While the maximum axial velocity is higher for the MIL propeller, peaking at around $0.75R$, the average axial velocity is higher for the LA propeller - $12.7m/s$ compared to $11.8m/s$ at distance $1R$ downstream from the propeller plane.

Furthermore, the development of the axial velocity profile downstream of the propeller plane was also compared. As per the actuator disk theory, the velocity is still increasing after the propeller plane, but the rate of increase is biggest directly after the propeller plane and then starts to decrease. It can also be observed that it is eventually smoothed out, namely the changes in profile gradients lessen which makes the profile of the LA propeller even more uniform, while the peak of the MIL propeller profile moves slightly towards the middle of the blade. This is consistent with the model presented by Khan and Nahon (2015), even though in the present case the wake expansion is not taken into account as the propeller is usually fairly close to the wing and inviscid flow is assumed.

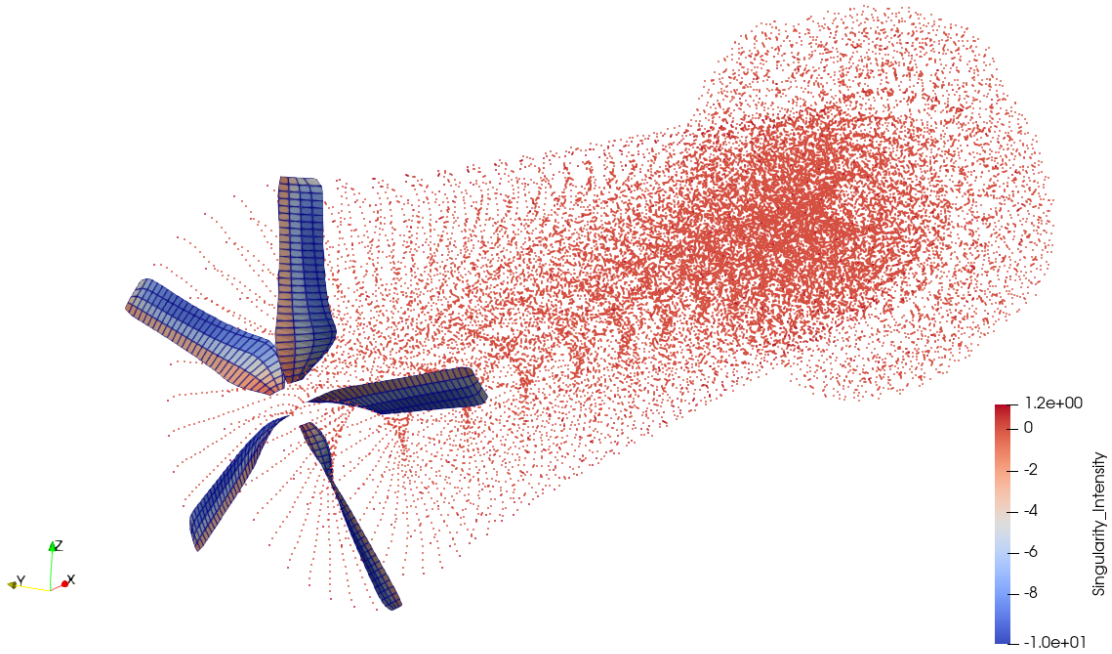

(a) LA propeller.

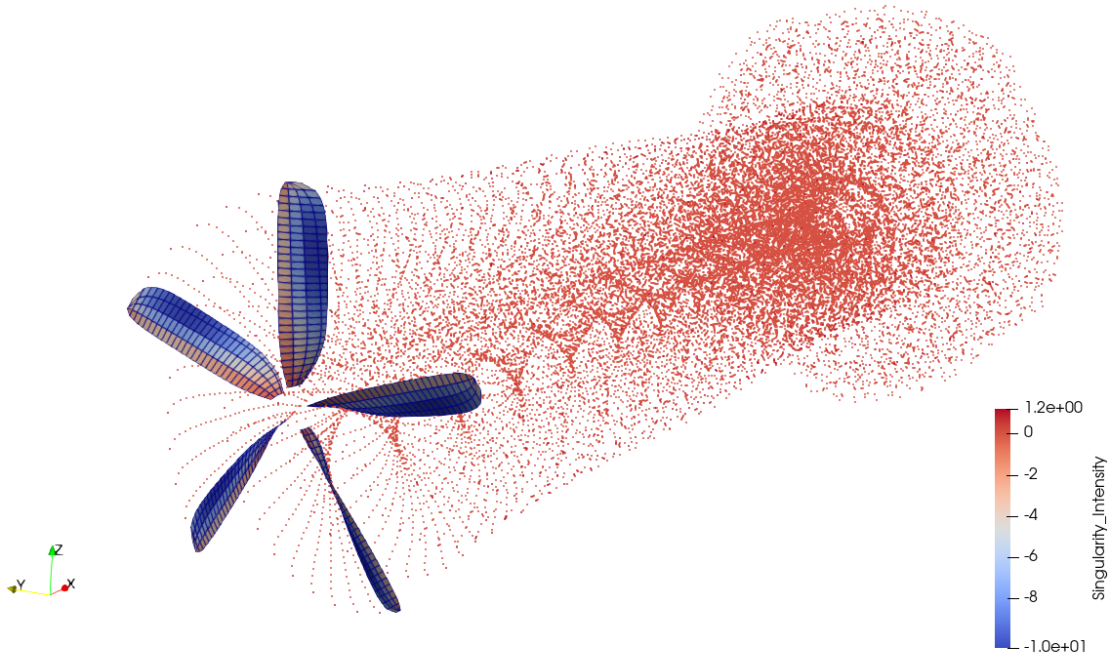

(b) MIL propeller.

Figure 3.8: Vortex lattice models of the LA and MIL propellers produced by DUST.

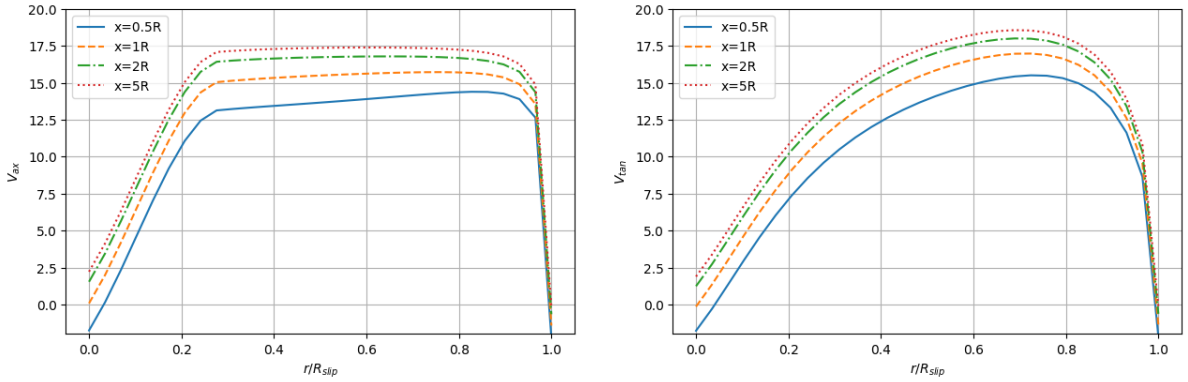

(a) Slipstream axial velocity profile for LA propeller

(b) Slipstream axial velocity profile for MIL propeller

Figure 3.9: Comparison of slipstream axial velocity profiles for MIL and LA propellers at different stations downstream; $J = 0.8$ and $C_P = 0.294$.

Next, the performance of the two propellers was compared. Firstly, the average axial slipstream velocity at distance 1R behind the propeller plane was analyzed with respect to advance ratio. Three pairs of LA and MIL propellers were designed, all were given the same input power but different design advance ratios. Then their offdesign performance was analyzed at different input powers. At a certain power level, a propeller's operation would correspond to a certain thrust and RPM (and hence advance ratio). The average axial slipstream velocity was then calculated at 1R behind the propeller plane. The results are presented in figure 3.10. It can be observed, that for individual design advance ratios the plots intersect at a certain point, meaning that after a certain advance ratio the MIL propeller will produce higher average axial slipstream velocity than the LA propeller. This point is in all cases at a slightly higher advance ratio than the design advance ratio of the propellers. The curves of MIL propeller are in general less steep than the ones of the LA propeller, meaning that the MIL propeller is less sensitive to changes in advance ratio and thus more versatile. However, in the range of lower advance ratios, which are more relevant for the take-off and landing phases of the aircraft's flight, the LA propeller produces higher average axial slipstream velocity. This shows, that an LA propeller actually present and advantage when compared with a MIL propeller in terms of lift augmentation, not only in terms of a more uniform slipstream axial velocity profile, but also by producing higher axial velocities in the slipstream, however only in the range of lower advance ratios. Above the crossover point, the MIL propeller is capable of producing higher average axial slipstream velocity.

By looking at figure 3.11 the difference in propulsive efficiency between the two propellers can be observed. For most of the analyzed advance ratio range, the efficiencies of the two propellers are very similar. However, as the higher advance ratios are approached the efficiency of the LA propeller starts to drop off more rapidly than the one of the MIL propeller. Paired with the fact that it also produces a higher average axial slipstream velocity than the LA propeller, it means that the MIL propeller is much more suited for higher advance ratios and thus higher freestream velocities. This bodes well for the DEP system in question which would primarily use all propellers during take-off and landing to augment lift and then only the MIL propeller during cruise to increase efficiency.

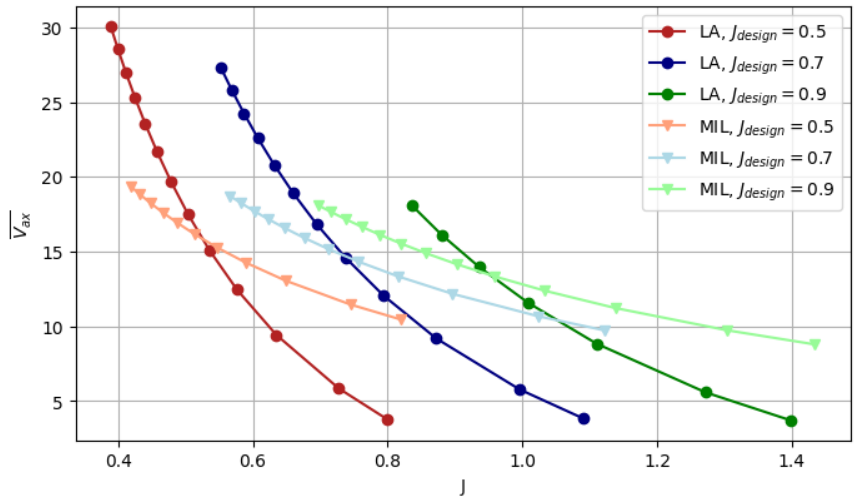

Figure 3.10: Comparison of average axial slipstream velocity at 1R behind the propeller plane for MIL and LA propellers at different advance ratios.

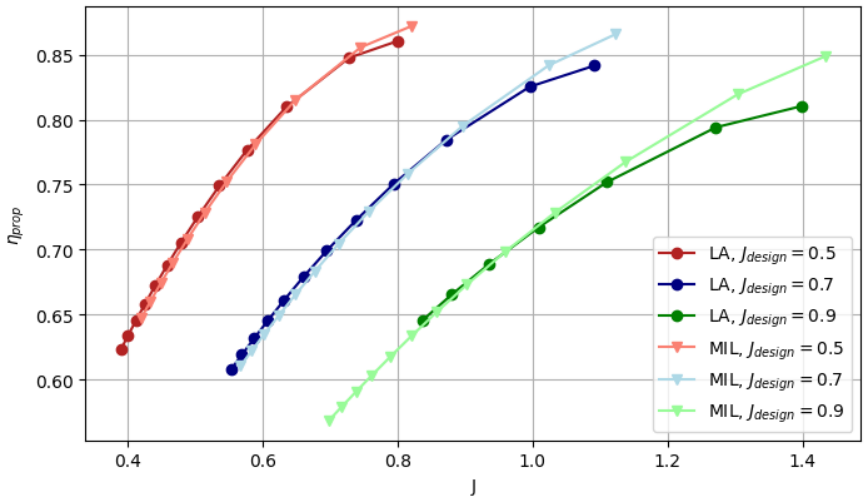

Figure 3.11: Comparison of propulsive efficiency for MIL and LA propellers.

4

DEP Design and Evaluation

4.1 Lifting Line Solver

At the core of this DEP evaluation tool is a lifting line solver based on the Fourier sine analysis adapted for the purposes of DEP evaluation. This is mostly represented in the addition of $(1+a)$ (defined in equation 4.1) to U_∞ and a contribution of propeller induced angle of attack α_{i_p} in the fundamental lifting line equation.

$$a = \frac{U_R}{U_\infty} - 1 \tag{4.1}$$

The induced velocity at point P at position $\mathbf{r}$ induced by an infinite vortex filament of circulation Γ can be calculated with the Biot-Savart law of induction.

$$\mathbf{V} = \int_{-\infty}^{\infty} \frac{\Gamma}{4\pi} \frac{\mathbf{dl} \times \mathbf{r}}{|\mathbf{r}|^3} \tag{4.2}$$

By combining the circulation contributions of all trailing vortices, the velocities (or rather downwash) in the wake at the spanwise position y_0 can be calculated.

$$w(y_0) = -\frac{1}{4\pi} \int_{-b/2}^{b/2} \frac{(d\Gamma/dy)dy}{y_0 - y} \tag{4.3}$$

The induced angle of attack α_{i_w} follows:

$$\alpha_{i_w}(y_0) = tan^{-1}\left(\frac{-w(y_0)}{U_\infty(1+\tilde{a})}\right) = tan^{-1}\left(\frac{1}{4\pi U_\infty(1+\tilde{a})} \int_{-b/2}^{b/2} \frac{(d\Gamma/dy)dy}{y_0 - y}\right) \tag{4.4}$$

With some fairly simple manipulation of the standardly defined angles, the fundamental equation of Prandtl's lifting line (equation 4.7) can be obtained.

$$cl = \frac{dC_L}{d\alpha}(\alpha_{eff} - \alpha_{L=0}) = \frac{2\Gamma}{U_\infty c} \tag{4.5}$$

$$\alpha_{eff} = \frac{2\Gamma}{(dC_L/d\alpha)U_\infty c} + \alpha_{L=0} \tag{4.6}$$

$$\alpha(y_0) = \alpha_{eff}(y_0) + \alpha_{i_w}(y_0) - \alpha_{i_p}(y_0) =$$
$$= \frac{2\Gamma(y_0)}{(dC_L/d\alpha)(y_0)U_\infty c(y_0)} + \alpha_{L=0}(y_0) + tan^{-1}\left(\frac{1}{4\pi U_\infty(1+\tilde{a})}\int_{-b/2}^{b/2}\frac{(d\Gamma/dy)(y_0)dy}{y_0 - y}\right) - \alpha_{i_p}(y_0) \tag{4.7}$$

In equation 4.7, the only unknown is the circulation Γ (or rather its distribution $\Gamma(y_0)$). In order to compute it, a Fourier sine series will be utilized. The main assumption of this procedure is that any circulation distribution can be represented as a sum of (infinitely) many scaled sine functions. The first step is to transform the spanwise coordinate y into θ where $0 \leq \theta \leq \pi$:

$$y = -\frac{b}{2}\cos\theta \tag{4.8}$$

Now the circulation distribution with respect to θ using the sum of the sine functions can be defined.

$$\Gamma(\theta) = 2bU_R\sum_1^n A_n \sin(n\theta) \tag{4.9}$$

Usually, there is U_∞ in the place of U_R however as we are also interested in the velocity contribution of the propellers this needs to be taken into account. This complicates things a little bit since $\vec{U_R}(\theta) = \vec{U_\infty} + \vec{u_a}(\theta) + \vec{u_t}(\theta)$ is now a function of spanwise position θ as can be seen in figure 2.3. By moving spanwise through a section of the wing washed by a propeller one would first observe an increase in velocity due to the induced axial velocity behind the first blade and either up- or downwash due to the tangential induced velocities, depending on the rotation direction of the propeller. At the center of the slipstream both of them go towards 0 due to the hub of the propeller. Lastly, as the area behind the other side of the propeller is approached the axial velocity increases again while the vertical velocity will be in the different direction compared to before.

The new definition of Γ from equation 4.9 can be inserted into the fundamental lifting line equation 4.7. All of variables that depend on y have to be transformed to the θ coordinate system. $d\Gamma/dy$ can be calculated individually.

$$\frac{d\Gamma}{dy} = \frac{d\Gamma}{d\theta}\frac{d\theta}{dy} = \frac{4U_\infty}{\sin(\theta)}\left(\tilde{a}'(\theta)\sum A_n\sin(n\theta) + (1+\tilde{a}(\theta))\sum nA_n\cos(n\theta)\right) \tag{4.10}$$

$$\alpha(\theta) = \frac{4b(1+\tilde{a}(\theta_0))\sum A_n\sin(n\theta_0)}{(dC_L/d\alpha)(\theta_0)c(\theta_0)} + \alpha_{L=0}(\theta_0) +$$
$$tan^{-1}\left(\frac{1}{\pi(1+\tilde{a}(\theta_0))}\int_0^\pi \frac{[\tilde{a}'(\theta)\sum A_n\sin(n\theta) + (1+\tilde{a}(\theta))\sum nA_n\cos n\theta]d\theta}{\cos\theta - \cos\theta_0}\right) - \alpha_{i_p}(\theta) \tag{4.11}$$

This is the final equation where the only unknowns are the Fourier coefficients A_n that can be calculated with a method like LU decomposition. The coefficients can than be inserted back into equation 4.9 to obtain the spanwise circulation distribution which can then be used to calculate lift and drag (coefficients) of the wing. Sectional lift and drag coefficients can however be obtained with a tool like XFOIL.

4.2 Thrust and Drag Book-Keeping

4.2.1 Induced Drag

Induced drag presents a big chunk of total drag, increasingly so at higher lift coefficients, for example, during the climbing phase. Furthermore, its reduction is deemed as one of the main benefits of DEP systems. For these reasons, it is important that it is included in the analysis and later in the optimization. Veldhuis (2005) presents an equation for the calculation of induced drag coefficient C_{D_i} for a wing with propellers in front of it, which can be easily evaluated after obtaining the Fourier coefficients from the Fourier analysis.

$$\begin{aligned} C_{D_i} = 2 \cdot AR \cdot \sum_n \sum_k n A_n A_k \int_0^\pi \sin(n\theta)\sin(k\theta)(1+\tilde{a}(\theta))d\theta + \\ 2 \cdot AR \cdot \sum_n A_n \int_0^\pi \alpha_{i_p}(\theta)\sin(n\theta)\sin(\theta)(1+\tilde{a}(\theta))d\theta \end{aligned} \tag{4.12}$$

4.2.2 Parasitic Drag

Veldhuis (2005) found out that the inclusion of viscous drag in the optimization procedure alongside induced drag impacts the final results considerably, making them more realistic. As the airfoil polars were already obtained from XFOIL, the $C_d(y)$ distribution can easily be obtained from the $C_l(y)$ distribution calculated from the circulation distribution $\Gamma(y)$. This way of calculation is quite simple, but it neglects some arguably important effects. Firstly, it only takes into account 2D airfoil polars, which are not completely representative of the 3D wing. Secondly, viscous phenomena are very difficult to predict even for an airfoil, let alone for a wing. The interference effects at the junctions of the wing and the propeller nacelles and fuselage were also not taken into account. However, as the main solver is of relatively low-fidelity and there are perhaps some even more influential assumptions made elsewhere, it was deemed that this simple method is of sufficient accuracy to be included in our DEP evaluation, although increasing the accuracy of viscous drag estimation would definitely be an interesting thing to look at in the future.

4.2.3 Nacelle Drag

Looking at it purely lift-wise, having multiple propellers seems like a great idea; however, from a drag (or maintenance perspective), it might not be so great, especially in cruise when the blades of the lift-augmenting propellers are meant to be stowed away as there is not a need for a lot of lift. Each additional nacelle produces extra unwelcome drag, which is not insignificant

and needs to be approximated somehow, so that the configurations with many lift-augmenting propellers do not appear too advantageous.

This procedure needed to be fairly computationally inexpensive so as to not take much extra evaluation time, so a surrogate model based on experimental data from Silverstein and Wilson (1939) was created. The model takes in the ratio of the nacelle diameter and the thickness of the wing behind it D_n/t_w, the length of the nacelle, and the lift coefficient of the wing and outputs an approximate value for the increase of C_D due to the presence of the nacelle. The experiment showed that the highest increase in C_D occurred when D_n/t_w was low, the nacelle was long, and the lift coefficient was high. This data was linearly interpolated and extrapolated to produce a quick method of nacelle drag estimation.

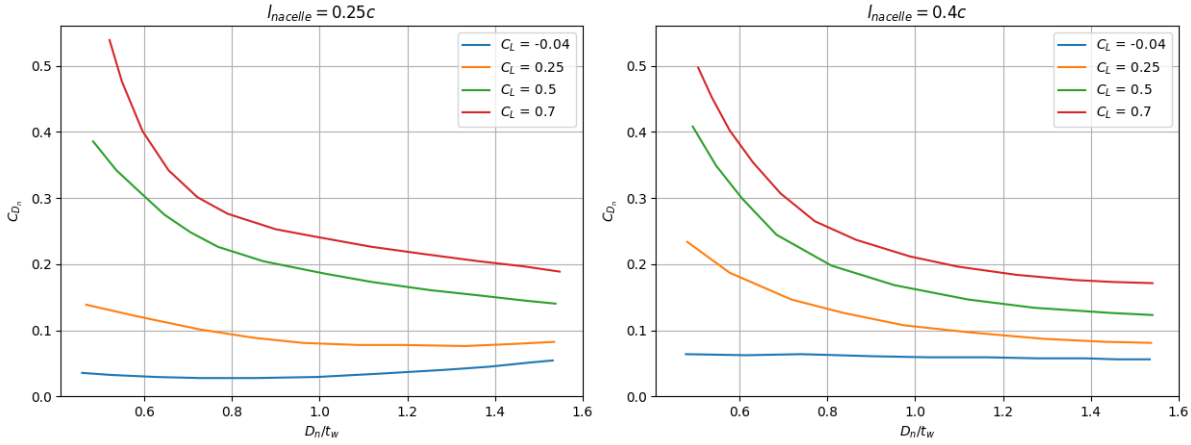

(a) Nacelle length $0.25c$

(b) Nacelle length $0.4c$

Figure 4.1: Nacelle drag coefficient experimental data from Silverstein and Wilson (1939).

It has to be noted that this is a very rough estimation. There are many potential sources of error from converting relatively old results from a wind tunnel to a surrogate model, and the validity of linear interpolation and, needless to say, extrapolation are very big assumptions. However, because of interference drag, accurate numerical simulation of nacelle drag contribution would also not be an easy feat. Therefore, because the main solver is of relatively low fidelity and there are perhaps some even more influential assumptions made elsewhere, it was deemed that this simple surrogate model is of sufficient accuracy to be included in our DEP evaluation, although increasing the accuracy of nacelle drag coefficient estimation would definitely be an interesting thing to look at in the future.

4.3 Lifting Line Solver Validation

Next, the predicted propeller performance can be used to generate the slipstream velocities behind it and superimpose them onto a lifting line. The results of this were compared to the experimental data from the PROWIM wind tunnel experiments of Veldhuis (2005). This study was chosen due to publicly available geometry and experimental data and because many other studies also used them as a reference so the results of the present work can also be quickly compared with them.

The experimental setups consist of a 4-bladed propeller (analyzed in chapter 3.3) with a diameter of 0.236 m and a straight half-wing with a span of 0.64 m and an aspect ratio of $A = 5.33$. The main difference between the PROWIM and the APROPOS experimental setups is that with PROWIM the position of the propeller relative to the wing is fixed while with APROPOS the propeller can be positioned and angled freely with respect to the wing, which allows for a more detailed analysis of the interaction between the propeller and the wing. The results of the comparison can be seen in the following figures.

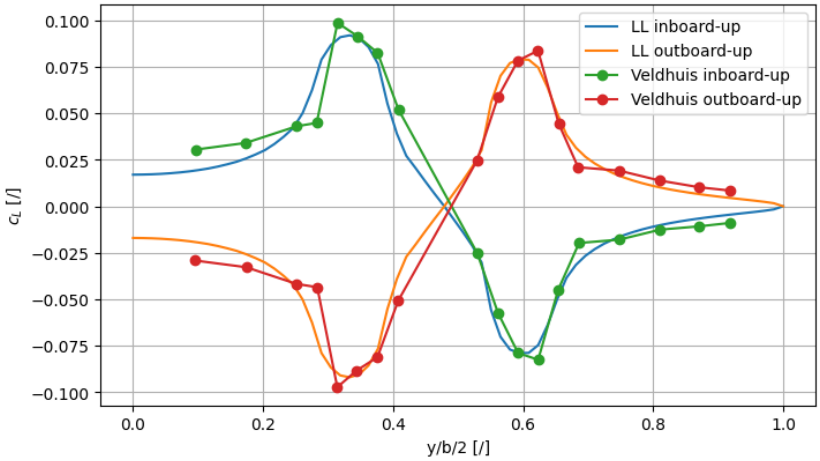

(a) PROWIM spanwise c_L distribution for $\alpha = 0°$

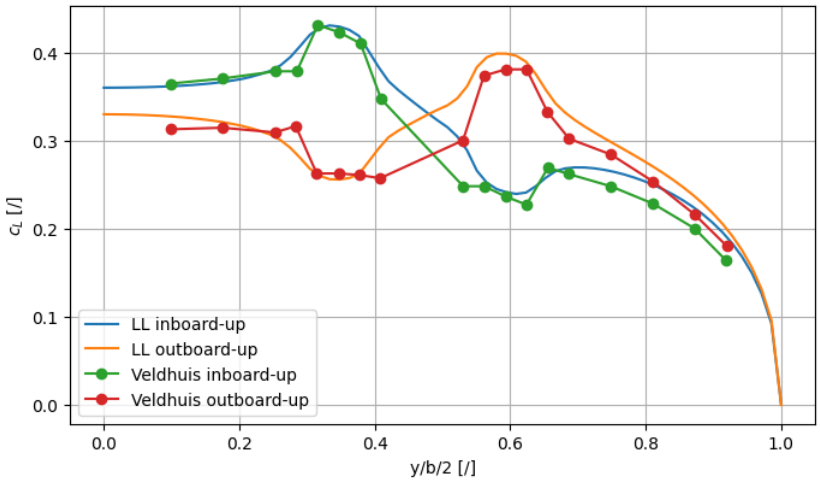

(b) PROWIM spanwise c_L distribution for $\alpha = 4°$

Figure 4.2: PROWIM spanwise c_L distribution comparison

Predicted lift distribution when the angle of attack is 0° is quite accurate. The largest deviation arises at the $y/b/2 = 0.0$, likely due to some junction and interference effects in the experiment which were not accounted for in the simulation because a mirrored symmetry was assumed. In the case of $\alpha = 4°$ the predicted lift distribution is off by a larger margin, which was also the case for similar numerical validation of the PROWIM setup. Here a big discrepancy arises at the position of the nacelle, which was not included in the lifting line model. As in the experiment, the geometry at that point is not suitable for lift generation, the lift distribution is lower than that predicted in the simulation.

4.4 Effect of Propeller Configuration on Take-Off Angle of Attack

In this section, the effect of the number of propellers on the performance of the aircraft is investigated. As one of the main purposes of DEP is to decrease the take-off distance of the aircraft, it was (indirectly) chosen as the comparison metric in this section. This was done by comparing the take-off angle of attack at different velocities for different numbers of propellers. If the take-off angle of attack is lower, consequently the take-off distance is also assumed to be lower.

The propellers were designed using Patterson's method for designing lift-augmenting propellers, which were found to produce higher average axial slipstream velocity and thus augment lift more than typical minimum induced loss propellers. The radii of the propellers were chosen such that the total propeller disk area is the same for all cases. Furthermore, the same was also done for the total propulsive power while the advance ratio of the propellers was also kept constant. The wing geometry was fixed for all cases and the propellers were evenly distributed across its span.

The take-off angle of attack was found using the bisection method for each individual free stream velocity and number of propellers by imposing vertical force equilibrium. This was checked by equating the weight of the aircraft to the sum of the vertical forces produced by the wing-propellers assembly. These include the lift produced by the wing, the thrust produced by the propellers in the vertical direction, and the normal force of the propellers due to their inclination angle with respect to the inflow velocity. The rate of climb was set to 0 m/s as the aircraft has not yet taken off and the atmospheric conditions were set to standard sea level conditions.

Firstly, only the influence of different numbers of propellers on the take-off angle of attack was investigated, so the vertical offset (z_R) and inclination (i_p) of the propeller were kept at 0. The results can be seen in figure 4.3. It can be observed that the take-off angle of attack decreases both with increasing number of propellers and with increasing free stream velocity. With increasing free stream velocity, it is naturally decreasing exponentially as the lift has a quadratic relationship with the velocity. However, the decrease in angle of attack with increasing number of propellers is also not linear. The biggest decrease in angle of attack is observed when going from 1 to 2 propellers, while increasing the number of propellers further has an ever smaller effect. The difference between 6 and 7 propellers is in most cases very small.

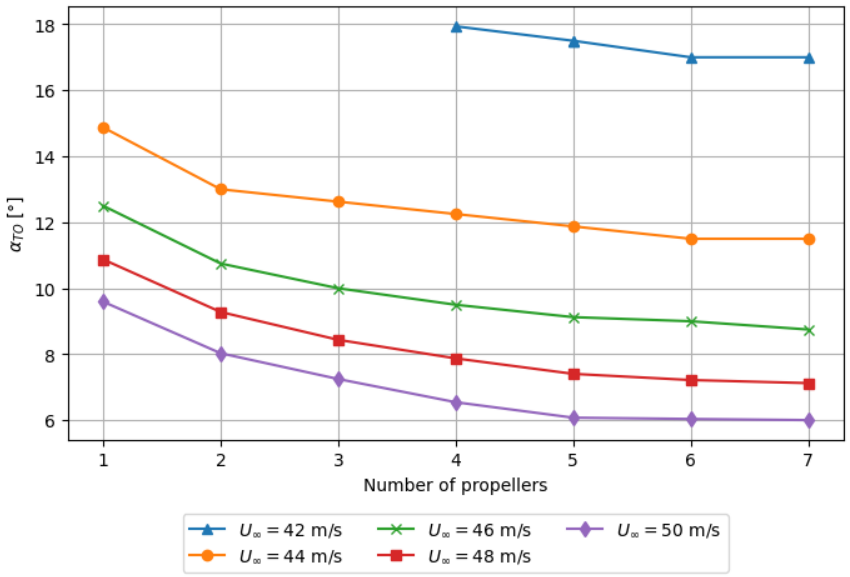

Figure 4.3: Take-off angle of attack at different velocities for different number of propellers.

This decrease in effect can also be nicely seen in figure 4.4 where the lift augmentation $C_L/C_{L,unblown}$ is plotted against the number of propellers and free stream velocities at the found take-off angles of attack. Again, the biggest difference is observed when transitioning from 1 to 2 propellers, however, increasing the number of propellers further does not increase the lift augmentation as much. One would naturally expect that the lift augmentation would be higher at lower free stream velocities, which is the case if the angle of attack is kept constant. However, as the take-off angle of attack is decreasing with increasing number of propellers, the lift augmentation is actually higher at higher free stream velocities. This points to the fact that the propellers do not increase the lift of the wing as much at higher wing angles of attack, due to the lift coefficient already being close to the peak of the lift curve. This is consistent with the results of Fei et al. (2018), who also found that the lift augmentation is higher at higher freestream velocities.

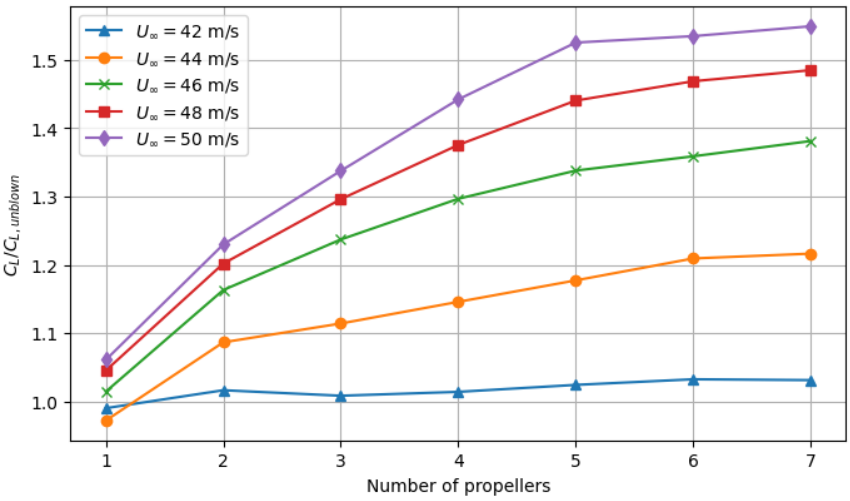

Figure 4.4: Lift augmentation at different velocities for different number of propellers at take-off angle of attack.

Next, the effect of the propeller inclination on the take-off angle of attack was investigated. The propellers were placed at $z_R = 0$ while i_p was varied from around -8 to 8 degrees. This was done at different freestream velocities for $N_{prop} = 5$. The results can be seen in figure 4.5. Contrary to expectations, it was observed that the take-off angle of attack actually decreases with increasing propeller inclination. It still holds that the lift augmentation is higher at lower propeller inclinations; however, downward-pointing propellers naturally produce some downward force, which counteracts the augmented lift caused by the increased local angle of attack of the wing. The balance between the two lift contributions depends greatly on the thrust coefficient of the propeller and the size of the wing in respect to it. Although it can be seen that the lowest take-off angle of attack is achieved at fairly high positive propeller inclinations, it does not make sense to use such high angles in practice because this way the component of thrust in the forward direction is greatly reduced, which would increase the take-off distance of the aircraft, which is the opposite of what is desired. But at least from this analysis, it can be concluded that if the propellers can be inclined, it would be better to incline them upwards rather than downwards since the reduction in thrust would be the same, but the vertical force would be increased. The reason why the minimum take-off angle of attack at lower free stream velocities is achieved at higher propeller inclinations is that because the wing has to operate at a higher angle of attack, the lift augmentation/attenuation is lower, and so the direction of the propeller thrust has a bigger effect on the take-off angle of attack. Similar results were also found by Fei et al. (2018) who concluded, that the optimal direction of inclination of a propeller likely depends on the specific configuration.

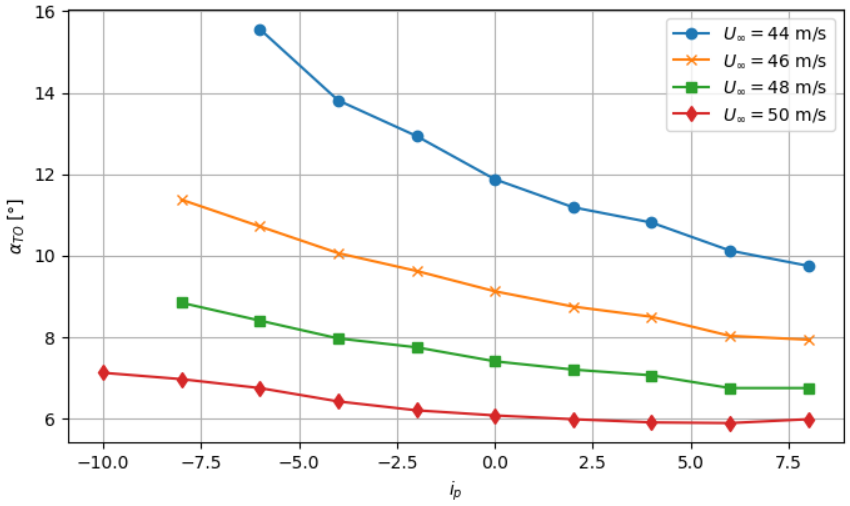

Figure 4.5: Effect of propeller inclination on take-off angle of attack at different velocities for 5 propellers.

The vertical offset of the propellers also has an effect on the take-off angle of attack. A similar study was done as with the propeller inclination; however, the propeller inclination was kept at 0 while the vertical offset was varied from -0.5 to 0.5 R. Here, the results are not so straightforward. As was found by Veldhuis (2005), at high thrust coefficients, the lift coefficient is higher if the propeller vertical offset is either slightly positive or negative. This happens because more of the wing gets submerged in the high dynamic pressure region of the slipstream. Furthermore, by submerging the wing in the bottom part of the slipstream, its contraction also slightly increases the local inflow angle of attack, which further increases lift. By putting the propeller-wing assembly at a certain angle of attack with respect to the

freestream velocity, the slipstream will be deflected to some degree, meaning that the wing will automatically be submerged lower in the slipstream than before. This results in the minimum CL being achieved at a slightly negative vertical offset. This manifests itself in the highest take-off angle of attack also being at somewhat negative vertical offsets. By increasing the free stream velocity or decreasing the thrust coefficient, the slipstream will get deflected more, and the peak of increased angle of attack will be achieved at ever lower vertical offsets, while the minimum angle of attack will be achieved at ever higher vertical offsets. The results can be seen in figure 4.6.

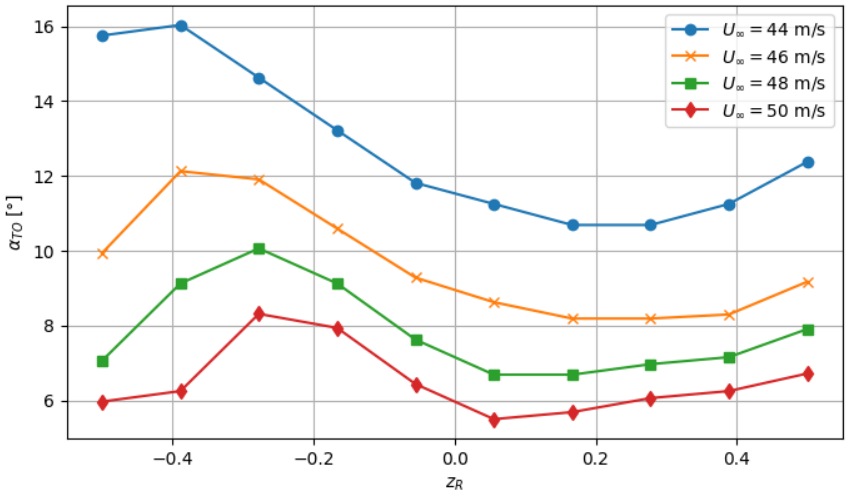

Figure 4.6: Effect of propeller vertical offset on take-off angle of attack at different velocities for 5 propellers.

5

DEP Optimization

5.1 Optimization Setup

The main optimization procedure focused on optimizing the aerodynamic performance of a Unifier19-like aircraft - a regional short-distance aircraft meant to accommodate 19 passengers plus a pilot (Unifier19, n.d.). Two main objectives that a good propeller configuration should achieve in terms of aerodynamic and propulsive efficiency are: 1) short take-off distance and 2) low power consumption during cruise (high efficiency). Three different configurations in terms of MIL propeller position were assessed:

1. One MIL propeller on the inboard side of each wing half with the main purpose of producing thrust and N lift-augmenting propellers on the outboard side of each wing half.
2. One MIL propeller on the tip of each wing half with the main purpose of producing thrust and N lift-augmenting propellers on the inboard side each wing half.
3. One MIL propeller on the tail of the aircraft with the main purpose of producing thrust and N lift-augmenting propellers on each wing half.

These three designs are fairly feasible and were also considered during the conceptual design phase of the Unifier19 aircraft. The main idea here is to have the MIL propellers dimensioned for cruise with variable blade pitch producing thrust at all times as efficiently as possible while the lift-augmenting propellers would only be engaged during take-off, climbing and landing phases of flight to augment lift. During cruise, when the need for lift and thrust is lower, the electric motors powering them would switch off and the blades would collapse, leaving only the nacelles. It has to be noted that in the case of the configuration number 3, the MIL propeller will only be evaluated with BEMT and will not be included in the lifting line solver.

The evaluation of each solution was done both under take-off and cruise conditions so as to find designs, that would have the shortest take-off distance but would also be power-efficient in cruise. The main requirement for the cruise regime is low drag, high efficiency of the MIL propeller and low noise emissions, while during take-off and climb the production of lift is of highest importance. The simulated take-off conditions differ from the cruise in that there is lower freestream velocity and different atmospheric conditions (density and kinematic

viscosity).

The operational values defined by the user are the following:

- number of lift-augmenting propellers on one side of the wing,
- configuration type ("inboard", "outboard", "tail"),
- freestream velocity during cruise,
- acceleration during take-off,
- mass of the aircraft,
- wing span,
- wing chord,
- take-off aircraft angle of attack,
- MIL propeller airfoils and their positions,
- LA propeller airfoils and their positions,
- MIL propeller spanwise position,
- MIL propeller take-off advance ratio,
- MIL propeller cruise advance ratio,
- wing flap deflection angle during take-off.

The values of the user-defined parameter used in the optimization cases can be found in Appendix A. Ideally, the number of propellers would also be an optimization variable, however the optimization algorithms selected can only handle continuous variables and thus the number of propellers, being a discrete value, is not suitable as one. The configuration type value specifies which of the three base configurations to use. The tail-positioned MIL propeller configuration was set up in such a way that the total disk area of the MIL propellers was the same as in the other two configurations, while the LA propellers were now spread across a bigger portion of the wing, allowing them to have a slightly larger radius. Mass of the aircraft is primarily used to calculate the required lift in both evaluated phases of flight and to figure out the required propeller forward thrust to achieve desired aircraft acceleration. The airfoils and their positions of all propellers also need to be specified. It was decided to lock in the position and advance ratios of the MIL propeller by the user as the focus of this thesis lies more in comparing different configurations of the LA propellers and in order to reduce the number of optimization variables as the optimization problem would quickly become too complex. Finally, as the emphasis of this research is to find the optimal propeller configurations it was decided to fix the wing geometry and make it simply rectangular. It was decided that the wing geometry would not be optimized, firstly, because the main focus of this research is on the propeller configurations and secondly, because it would complicate the optimization process and make it harder to observe the direct effect of the propeller configuration.

At this point some assumptions about the take-off procedure will be made to simplify the optimization. Firstly, it will be assumed that the take-off velocity is quadratically proportional to the take-off distance. It has to be acknowledged, that this is a fairly big approximation, however here is why it was deemed sufficient to make it. The take-off distance is a function of the take-off velocity and the acceleration of the aircraft. The acceleration is a function of the

thrust, aerodynamic drag, rolling resistance and the mass of the aircraft. The rolling resistance and mass of the aircraft will be assumed constant for all evaluated solutions. Furthermore, as the fuselage and wing designs of the aircraft are also kept the same the aerodynamic drag of the aircraft should also be fairly similar for all solutions at equal velocity. Thus the only variable that will be different for each solution is the thrust, which will be constrained to a value that will overcome the drag and achieve certain acceleration right before the take-off. From this it can be inferred that aircraft designs, which produce a high enough thrust and adequate lift coefficients will be able to take-off at lower velocities and thus shorter distances.

Secondly, the take-off angle of attack will also be deemed constant and the rotation phase of the aircraft will be neglected. A take-off angle of 10° will be used as most aircraft will not yet encounter a tail strike at this angle. Thus, if an aircraft is able to achieve lift-off at lower free-stream velocity the optimization algorithm will treat it as being able to take-off from a shorter runway. The cruise angle of attack will be found using bisection with the goal of achieving force equilibrium in the vertical direction.

Lastly, it has to be kept in mind that the goal of this optimization procedure is not to find the one "optimal" design, but rather to analyze the interplay between the different variables that influence the performance of a DEP system. Because many different assumptions were made throughout the propeller design and evaluation process, DEP system analysis and lastly its optimization, the absolute values obtained at the end of the optimization should be taken with a grain of salt. However, the relative differences between the different configurations should be fairly accurate and can be used to draw conclusions about the influence of different propeller configurations on the performance of a DEP system.

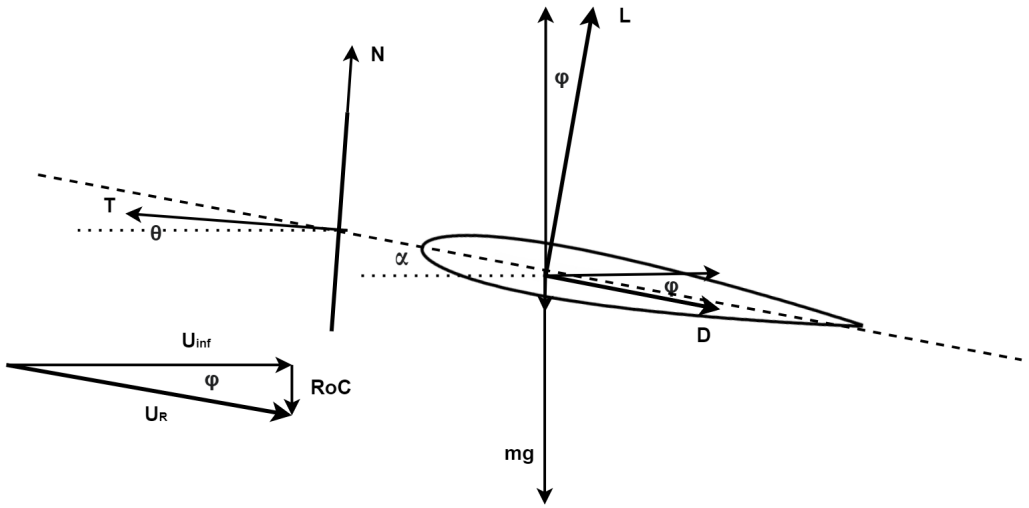

Figure 5.1: Schematic representation of the optimization problem.

Below is a list of the variables, that were decided to be optimized:

- take-off free stream velocity - $U_{\infty,TO}$,
- propeller forward distance with respect to the wing relative to the propeller radius - x_R,
- propeller vertical distance with respect to the wing relative to the propeller radius - z_R,
- propeller inclination angle with respect to the wing - i_p,

- LA propeller power during take-off - $P_{LA,TO}$,
- LA propeller advance ratio during take-off - $J_{LA,TO}$,
- MIL propeller radius - R_{MIL},
- MIL propeller power during take-off - $P_{MIL,TO}$,
- MIL propeller collective blade pitch during take-off - $\beta_{MIL,TO}$.

The relative propeller forward offset x_R (see figure 5.2) was decided to be bound downwards to 1.0, because one of the main design features of the DEP configuration being analyzed in the present work are the folding blades of the LA propellers and an offset of $1R$ is needed for that. The optimized z_R and i_p were only used for LA propellers while they were fixed to 0 and -3° for MIL propellers for simplicity respectively. In the current setup the radii and the spanwise positions of the LA propellers is calculated so that they cover most of the available span either inboard or outboard of the MIL propeller. The powers of both LA and MIL propellers and the advance ratio of LA propellers also need to be determined. As the LA propellers will primarily operate during take-off and climb stages of the flight they are designed to be as efficient as possible in those flight regimes, but because their geometry is fixed they probably would not perform as well in the cruise phase. However the MIL propeller is dimensioned for cruise and because it also has to provide some thrust during take-off its collective blade pitch can be adjusted by the optimization algorithm in order to be able to always achieve adequate efficiency.

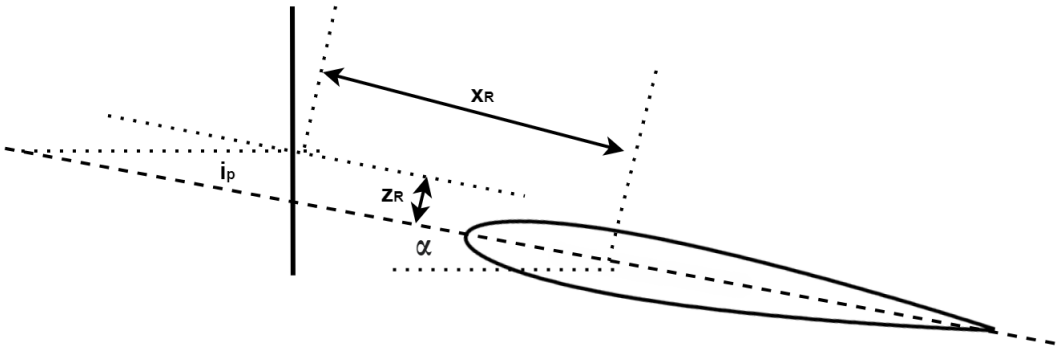

Figure 5.2: Schematic representation of propeller position definition.

The starting point of the optimization is a simple force equilibrium in the X and Y directions from the figure 5.1:

$$-T\cos\theta + N\sin\theta + L\sin\varphi + D\cos\varphi = 0 \quad \text{(X)} \tag{5.1}$$

$$T\sin\theta + N\cos\theta + L\cos\varphi - D\sin\varphi - mg = 0 \quad \text{(Y)} \tag{5.2}$$

Drag in the upper equations consists of the wing induced drag, wing parasitic drag, fuselage parasitic drag and nacelle drag. The optimization was set in such a way that $RoC = 0$ in both evaluated phases of flight so the equations become even simpler, however it can be of other values to evaluate the aircraft during climb, for example. These are the first two constraints of the optimization, namely that the sum of the forces taken into account has to be 0 during

cruise and some positive amount that corresponds to a predefined horizontal acceleration during take-off. A small margin of 2% was allowed as it would be impossible for the optimization algorithm to find a combination of optimization parameters where the left-hand-sides of the upper two equations equal exactly 0. The final constraint bounds the maximum chord length of the propeller blades to within $0.1R$ and $0.3R$ of the propeller so they are, at least in this sense, manufacturable.

The optimization also has two objectives. The first one will be, as stated before, the minimization of take-off distance/velocity, while the second one will be minimization of required power in cruise, which directly corresponds to increase of efficiency.

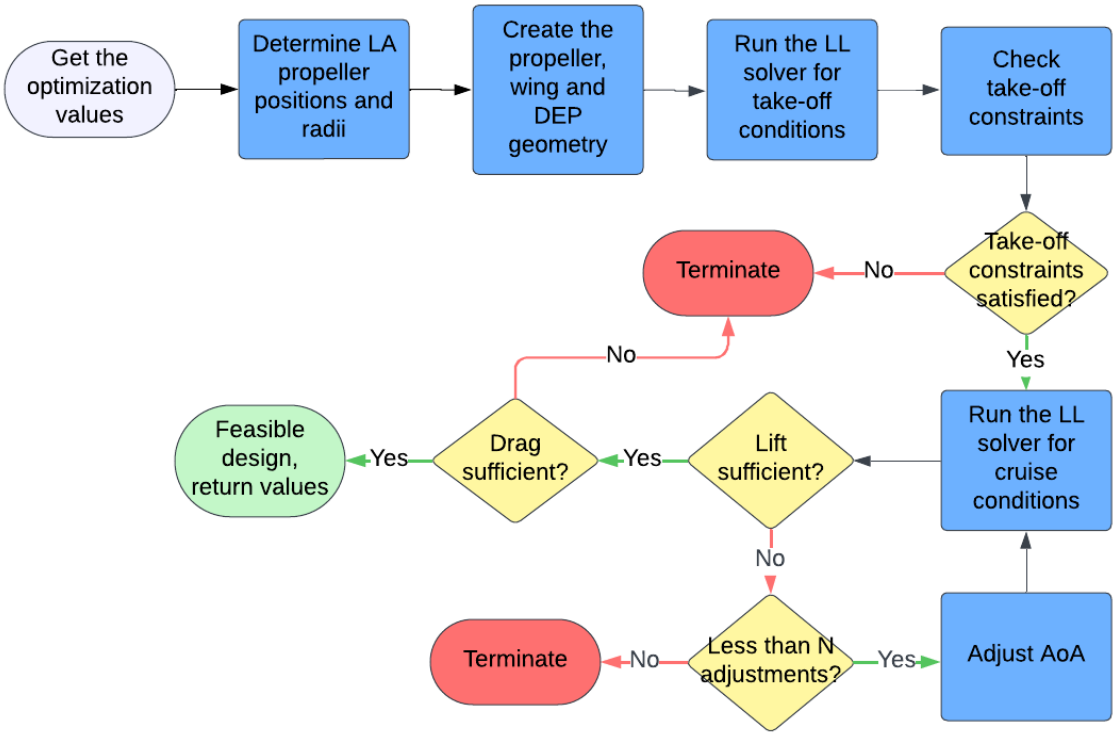

Figure 5.3: Simplified flowchart of the DEP feasibility evaluation function of the optimization procedure.

The objective function, constraints and the objectives of the optimization are packaged into a single function that evaluates each design and returns the values for constraints and objectives. A simplified flowchart of its action sequence is presented in figure 5.3. First, the optimization algorithm determines the values for the optimization variables. The span of the wing that is not occupied by the MIL propeller gets uniformly filled with N_{prop} equal LA propellers on each side of the wing. Now the geometry of the wing and the propellers can be created. LA propellers are designed at take-off conditions according to the Patterson's procedure while the MIL propeller geometry is generated for cruise conditions following the theory of Larrabee. The RPM's of propellers can also be determined at this point. Next, the configuration gets evaluated with the lifting line solver under the climb conditions. If the solution is infeasible, meaning that it does not satisfy the constraints, the procedure is terminated. In the case that it manages to satisfy the constraints, it is then once again evaluated with the lifting line solver,

but under the cruise conditions. Here an iterative scheme with bisection has been employed in order to find the angle of attack of the aircraft that satisfies the lift constraint. After it does, the evaluation concludes and the constraint and objective values are returned to the optimization algorithm.

In order to include the drag contribution of the fuselage it was modeled in an open-source parametric geometry development tool developed by NASA called OpenVSP. Being parametric, it allows for easy changes in the geometry of the fuselage which is useful for initial stages of design and analysis. An approximate recreation of the Unifier19 fuselage was drawn and analyzed for parasitic drag at both take-off and cruise conditions at different angles of attack. A function was created which would output the drag coefficient component of the fuselage for a given operational point. It has to be noted, that simply adding different drag components together is by no means a perfect way to calculate the total drag of the aircraft, however it should give a good enough approximation for the purposes of this research.

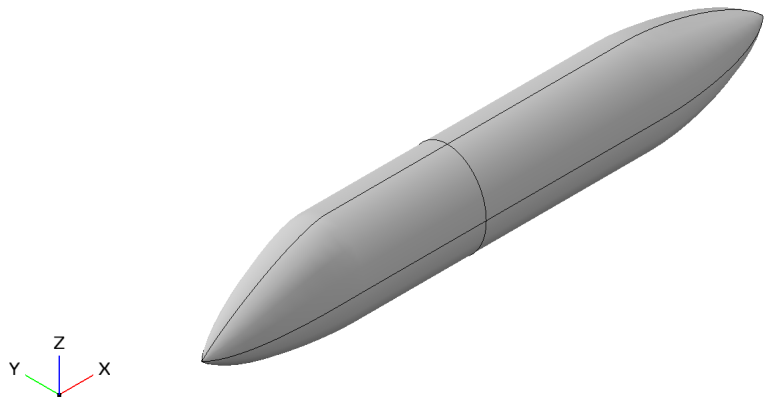

Figure 5.4: OpenVSP fuselage model.

5.2 Optimization Variable Correlation

Before looking at the results of the optimization it is important to understand how and to what degree different optimization variables influence the performance metrics of the DEP system. In order to do this a correlation analysis was made.

The variables, that were decided to be optimized were sampled using a latin hypercube sampling method that distributes the samples evenly across the design space. The number of samples was set to 1000. The samples were then evaluated using the same evaluation function as in the optimization procedure. The main difference between this and the optimization procedure is that in the optimization, the algorithm tries to narrow down on the best results based on the objective function, while in the correlation analysis the entire design space is explored, looking at how the different variables influence the performance metrics.

After all of the samples were evaluated, the correlation between the optimization variables and the performance metrics was calculated, producing a correlation matrix. A correlation matrix is a square matrix that shows the correlation between each pair of variables. A correlation

coefficient is a value between -1 and 1 that shows how much two variables are related. A value of 1 means that the two variables are perfectly correlated, a value of -1 means that the two variables are perfectly inversely correlated and a value of 0 means that the two variables are not correlated at all. The appropriate values were extracted from the correlation matrix and plotted in a heatmap presented in figure 5.5. All of the variables being optimized are on the x-axis, while the constraints and objectives (written in bold letters) of the optimization are on the y-axis. All of the constraints are presented in pairs since they had to insure that the values were within a certain range, so an upper and lower limits had to be set. It can be observed that within a pair the correlation is always exactly the same, but one of the constraints is always positively correlated with the optimization variable, while the other is negatively correlated.

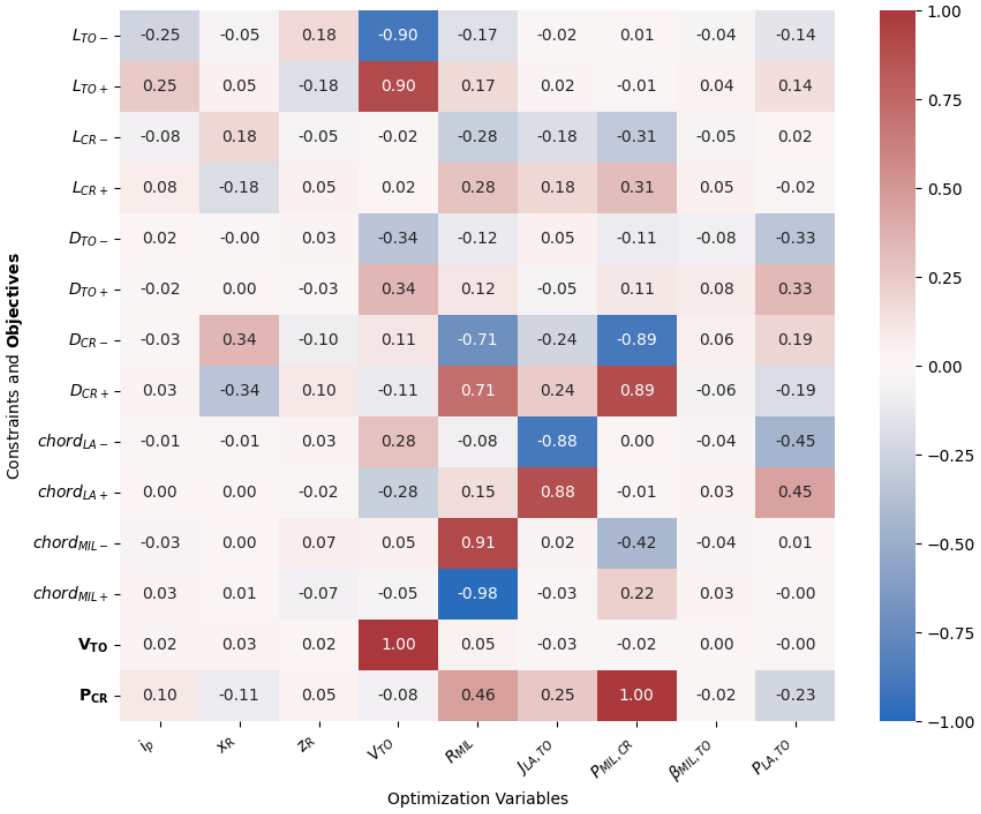

Figure 5.5: Correlation heatmap.

By first observing the influence of of the optimization variables on the first objective, the take-off velocity, it can be observed that there is naturally perfect correlation with itself, as it was set as one of the optimization variables. Other optimization variables actually do not seem to make a big influence on the take-off velocity. Values in the order of couple of percent can be deemed as errors, which could be avoided by running an even higher number of cases. By looking at the influence on the second objective, the cruise propulsive power, it can be observed that more variables have a significant effect on it. The highest is of course the input propulsive power. It is followed by the radius of the MIL propeller and as can be seen from the cruise drag constraints, there is a high correlation between cruise drag and the radius of the propeller, so it makes sense that the radius of the propeller would also have a high correlation with the cruise power.

The next two variables that significantly influence the consumed power during cruise, and

are also somewhat connected, are the advance ratio and the power of of the LA propellers during take-off. It can be inferred that both increasing the the advance ratio and decreasing their power contribute to reduced thrust produced by the LA propellers, meaning that more of it will have to be produced by the MIL propeller during take-off. Because the $J_{MIL,TO}$ and R_{MIL} are fixed beforehand, this leaves the increase in the average chord distribution or the collective blade pitch of the propeller as the two ways to increase the thrust produced by the MIL propeller. However, the former also influences the performance of the propeller during cruise, namely increasing the consumed power. As can be seen from the upper figure, this has a significant effect on the lift and drag during cruise. Due to the variable collective blade pitch of the propeller, this setting does not have an influence during cruise.

By looking at which optimization variables influence take-off lift, it can be observed that, expectedly, the take-off free stream velocity dominates. The propeller inclination angle has a positive correlation with the take-off lift, confirming the findings from chapter 4.4. The vertical offset of the propellers is somewhat negatively correlated with the take-off lift. In chapter 4.4 it was observed that it is better to position propeller slightly above the wing to reduce the take-off angle of attack, however the biggest difference with the analysis of this chapter is that before this was observed with 0° propeller inclination. In the current study, the combination of the two, together with the forward propeller offset, presents a much more challenging problem to analyze. The last two variables, that have a more or less significant influence on the take-off lift are the MIL propeller radius and the power of the LA propellers during take-off. Only two variables have a significant influence on the drag during take-off: the take-off velocity and the power of the LA propellers during take-off.

The variables that have a noteworthy influence on the cruise lift are the propeller forward offset, radius and power of the MILL propeller and the advance ratio of the LA propellers during take-off (discussed above). The first is negatively correlated, which means that it is better to have it closer to the wing, lift-wise. However, this might not always be so straightforward. By positioning the propeller further from the wing the average slipstream velocity will increase, but its diameter will decrease. Both of these effects affect lift. Furthermore, if the wing is at a high angle of attack, having the propeller further from the wing will also make the slipstream travel higher with respect to the wing, in extreme cases bypassing it alltogether. The i_p and z_R also have to be taken into account. The MIL radius and power have a positive correlation with the cruise lift. All of these variables also have a notable influence of the cruise drag, all of them being even more correlated with the drag than with the lift, which is the main driver for increased MIL propeller power during cruise.

Figure 5.5 gives a nice segue into the final optimization, giving some idea of what to expect.

5.3 Optimization Results

This chapter will present the results of optimization, meant to find DEP configurations that would allow and aircraft to take off in the shortest distance possible and to consume least power during cruise. Two different popular optimization algorithms were used, namely the genetic algorithm NSGA-II and the particle swarm optimization algorithm SMPSO. All DEP configurations included 5 lift-augmenting propellers on each half of the wing, however they differed in the position and number of the minimum induced loss propellers, meant mainly for

producing trust during cruise (see section 5.1).

The subsequent sections will systematically present the results of the optimization process and their implications. Firstly the results of one optimization case will be looked at in detail. Next, the results of the comparison between the three aircraft configurations will be presented. Finally, the comparison between the two optimization algorithms will be presented.

All optimizations were run on ona a 1.9 MHz, 12 core machine with 8 GB of RAM. Each solution of a generation was run on a separate core with the use of multiprocessing. Each optimization case took on average 17 hours to complete, evaluating 1600 configurations, which makes the average run time of one configuration evaluation around 38 seconds. It should be noted, that some of the configurations were deemed infeasible at different points in the evaluation process, which was subsequently terminated, reducing the average run time of one configuration evaluation.

5.3.1 Optimal Designs

In this chapter the general trends of the best designs of all optimization cases are discussed. Even though configurations with different positions of the MIL propeller were tested and with different optimization algorithms, the design directions turned out to be fairly similar. Following is an overview of how all each optimization variable behaved in the optimization problem at hand and influenced the final results.

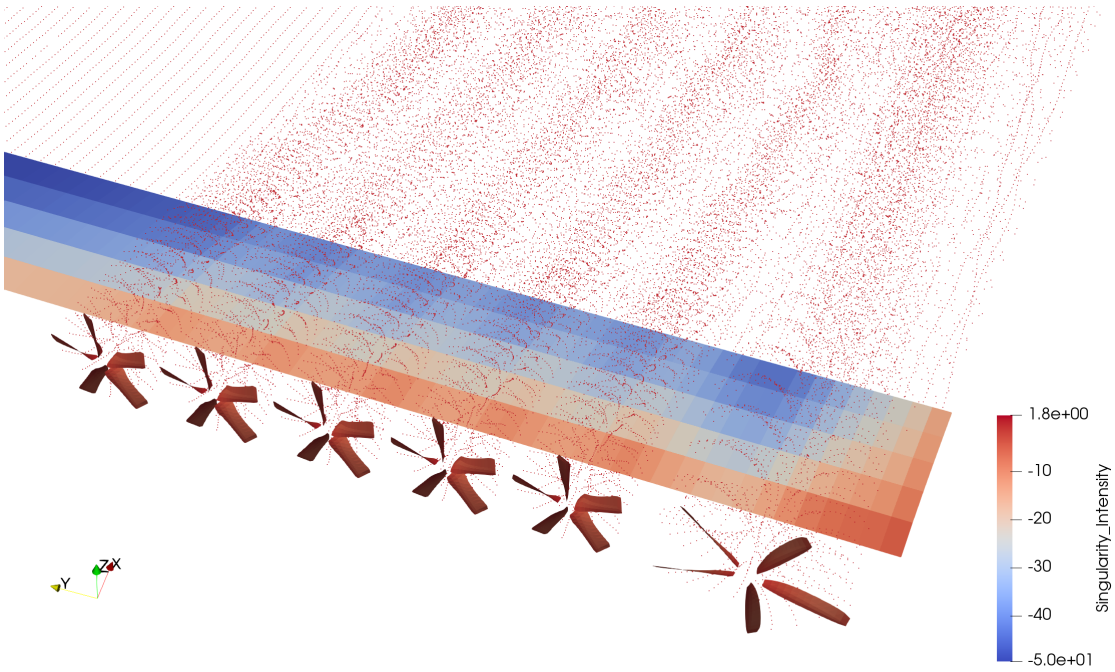

Figure 5.6: Visual representation of one of the designs on the Pareto front with an outboard positioned MIL propeller.

Firstly, the forward offset of the propeller with respect to the wing, x_R, was found to converge towards the lower set value of 1.0. Because of this, a few cases were run with unrestrictive bounds in order to check if there exists an even better solution with regards to the selected objectives and the x_R settled in the range from 0.5 to 0.7 for all cases. As was observed from

the correlation case, the forward distance of the propellers has a slight positive correlation with the cruise power, which means that the propellers should be positioned closer (to a certain extent) to the wing to reduce the power consumption during cruise.

The LA propeller inclination angle with respect to the wing, i_p, in all cases ended up at the upper bound of 8°. This result is on par with results from chapter 4.4, where it was found that positive propeller inclination would result in a lower take-off angle of attack at same velocity. Other studies have found mixed results on this topic, for example te experimental study of Fei et al. (2018) found similar results to the ones presented here, namely that with an increase in propeller inclination angle the $C_{L,wing}$ decreases but the $C_{L,eff}$ increases, while the study of Takallu and Gentry (1992) found that the effective lift coefficient $C_{L,eff}$ decreases with an increase in propeller inclination angle. From this it can be reasoned, that the final behavior of the propeller-wing system with regards to i_p is somewhat dependent of the specific configuration settings. Fei reckoned, that if a propeller is paired with a small wing with a shallow $c_L - \alpha$ slope, the $C_{L,eff}$ is likely to be positively correlated with i_p, because the thrust component in the direction of lift will be larger than the loss of wing lift due to smaller local angle of attack. The opposite would be true if a smaller propeller is mounted in front of a large wing with a steep $c_L - \alpha$ slope.

The vertical offset of the LA propellers with respect to the wing, z_R, was found to converge towards a slightly positive value of 0.2. The benefit of a positive vertical offset was already observed in chapter 4.4, where it was found that the take-off angle of attack could be reduced by positioning the propeller slightly above the wing.

In case the MIL propeller was positioned on the wing, its radius converged to around 1.7 R of the LA propellers, making it significantly larger. This is of course due to the need for thrust during cruise, which is the main purpose of the MIL propeller. However, if the MIL was situated on the tail of the aircraft its radius was almost exactly the value that produces the same total MIL propeller disk area as in the case where it was positioned on the wing.

The advance ratio of the LA propellers during take-off, $J_{LA,TO}$, settled in most optimization cases around 0.55. In the correlation study it was found that it negatively affects the drag and power during cruise, however a certain thrust is needed to accelerate the aircraft and bring it up to take-off velocity.

The collective pitch angle of the MIL propeller during take-off, $\beta_{MIL,TO}$, was found to converge to around -8°. This ensured that the MIL propeller operated efficiently even during the off-design conditions of take-off.

5.3.2 Effect of MIL Propeller Position

With the implemented DEP configuration evaluation models, the optimization algorithms were not able to find designs with inboard or outboard positioned MIL propeller that would have a noteworthy difference in the take-off velocity or the consumed power during cruise. On average, the values of the optimization variables of the solutions on the pareto front were fairly similar, regardless of the MIL propeller position. The differences were so small that they could easily be attributed to discretization errors. In order to verify this some of the solutions were recreated in the DUST solver. The results can be seen in section 5.3.4.

As for the tail configuration, there was a discernable difference. Interestingly, because the MIL propeller was not mounted on the wing, the lift augmentation was not as high and it could only take-off at higher velocities, about 2% higher. Also, because of the same reason, there was no lift augmentation at all during cruise and the angle of attack of the aircraft had to be around 10% higher, which in turn increased the drag and power consumption during cruise. There was also no added benefit of induced drag reduction, because the propeller was not mounted on the wing. It has to be kept in mind that the take-off procedure was greatly simplified in the optimization process and that the results should be analyzed with used approximations in mind.

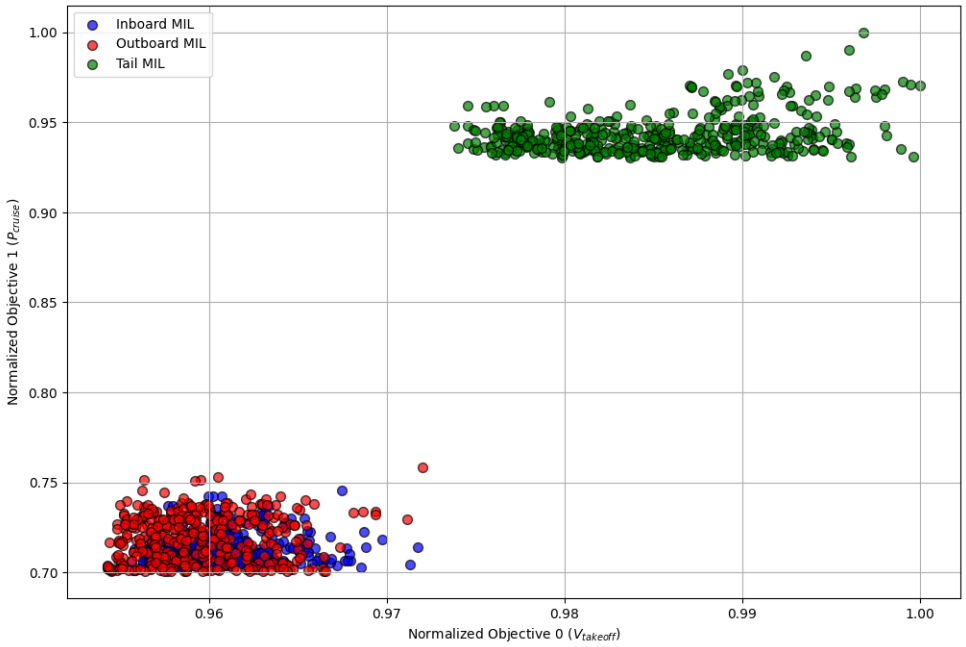

Figure 5.7: Comparison of the three DEP configurations.

As can be seen from figure 5.7, the consumed power during cruise for the tail MIL configuration is significantly higher. This can be attributed to higher predicted induced, parasite and nacelle drag.

5.3.3 Comparison of Optimization Algorithms

NSGA-II and SMPSO are fundamentally different optimization algorithms. NSGA-II is a genetic algorithm, which uses a population of solutions and evolves them over a number of generations. SMPSO on the other hand is a particle swarm optimization algorithm, which uses a number of particles to explore the design space by altering their positions and velocities. The optimization cases were run with identical settings so as to ensure a fair comparison between the two algorithms.

Both require some tuning of the parameters to work optimally. For the NSGA-II both mutation and crossover eta was set to 20, which is a good compromise between exploration and exploitation, while for the SMPSO algorithm mutation eta was set to 20, mutation probability to 0.9, mutation ratio to 0.15 and the range of both cognitive and social parameters was 1.5 - 2.5. The inertia weight range was set to 0.1 - 0.9.

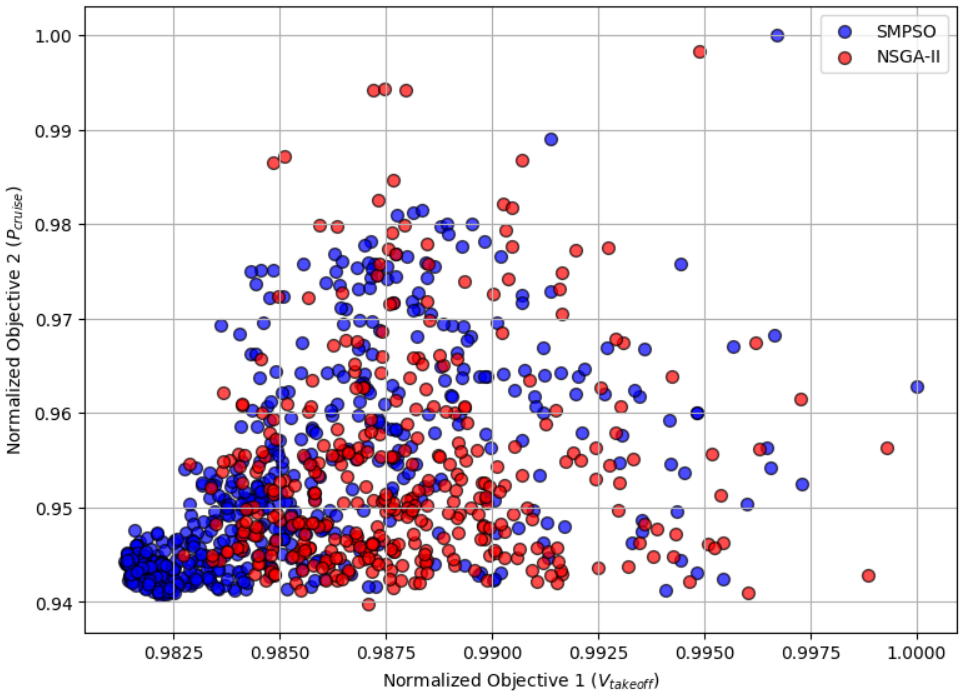

Figure 5.8: Comparison of NSGA-II and SMPSO optimization algorithms for inboard MIL configuration.

By looking at figure 5.8 it can be observed that the SMPSO algorithm converged faster towards the pareto solutions and managed to explore that area in much more detail. NSGA-II on the other hand, had a harder time converging towards the pareto solutions and kept exploring other areas. Because of these findings, some cases were run with larger mutation and crossover etas which promote exploitation, however in that case it would sometimes get stuck in a local minima and would likewise not manage to reach the pareto front as well. It was also observed that on average SMPSO managed to find feasible solutions quicker and thus had a chance to exploit the design space more. Moreover, if a too low mutation and crossover etas were selected, the mean of the objective values in each generation would not converge, since the algorithm would force the population to explore the design space more.

One of the biggest challenges of setting up these optimizations was the setup of the bounds and the initial population, especially when using the NSGA-II algorithm. If there were no feasible solutions in the initial population, the algorithm had a hard time finding them in the subsequent generations. This was less of a problem with SMPSO, however convergence was still much quicker if the inputs were set up correctly.

In the end, using appropriate settings, both algorithms managed to find fairly similar solutions, however SMPSO converged faster to the pareto front and managed to explore it in more detail. Direct comparison of the two algorithms is difficult, since they are fundamentally different and the selected parameters influence their behavior greatly. However, in the case of the present work, SMPSO was found to be more suitable for the optimization of selected problem.

5.3.4 Comparison with DUST

Some of the solutions on the pareto front were recreated in a mid-fidelity aerodynamic solver DUST to check the validity of the results. The propellers were modelled using a non-linear vortex lattice method (includes prescribed polars), while the wing was modelled using a regular vortex lattice. They were run for 13 revolutions of the LA propellers, which lasted around 1 hour and 30 minutes. Due to the number of propellers, the problem is quite a complex one, increasingly so with time, since the number of wake points is ever increasing.

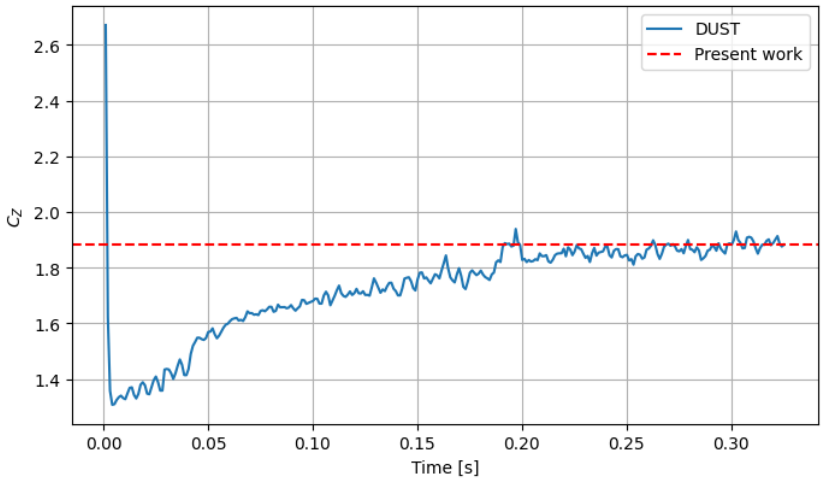

(a) Resultant vertical force coefficient (equivalent to C_L).

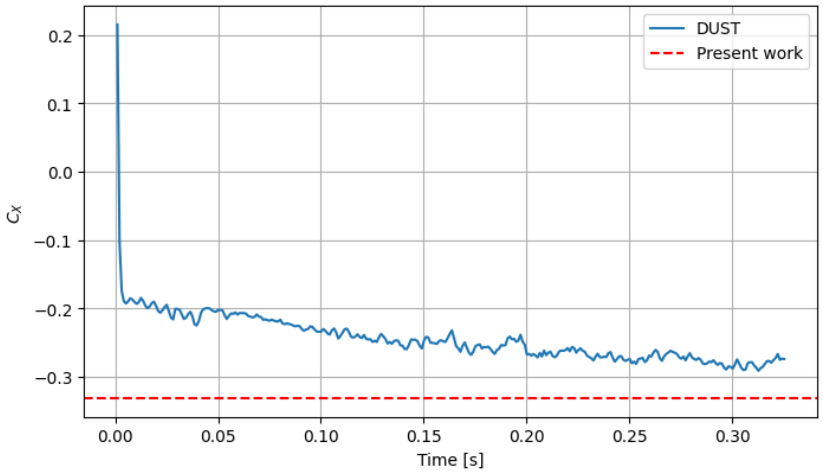

(b) Resultant horizontal force coefficient (equivalent to normalized drag minus thrust horizontal component).

Figure 5.9: Comparison of the total vertical and horizontal force coefficients of one of the optimal designs with the DUST results during take-off for an inboard MIL propeller configuration.

In the figure 5.9 the evolution of the resultant of vertical and horizontal forces can be observed and compared with the result provided by the optimization. As can be seen, after the forces settle down around the 0.25 s mark the lift coefficients are fairly similar, however the horizontal forces are slightly off. After the postprocessing of each individual component it was observed that the drag of the wing was estimated similarly, however DUST predicted somewhat lower thrust, which resulted in lower total forward force. This could be attributed to the use of different polars for the two simulations, because DUST used CFD-generated polars for the

MH114 and MH117 airfoils, while the BEMT solver developed in the present work used XFOIL's, which are likely not as accurate.

A flow field analysis was done for a take-off scenario of one of the optimal designs with an inboard MIL propeller configuration. In figure 5.10 some of the slices representing velocity magnitude at certain stations along the x axis can be observed (wing leading edge is located at $x = 0$). First slice is thus 10 cm in upstream of the leading edge and the second slice is at about $0.63c$ of the wing. The wake of the 12 propellers can clearly be seen, as well as the difference in velocity between the top and bottom surfaces of the wing in the first two slices and the velocity deficit in the wingtip vortex in the last three slices. There is also a noticeable downwash of the wakes as they move farther from the wing, due to the high angle of attack of the wing. It is interesting to note that the wing has a lot of effect on the flow field even in front of the leading edge. For some reason, DUST predicts that the velocity magnitude in the slipstream of the propeller next to the MIL propeller is noticeably lower than in the slipstreams of the other propellers. It would appear that the MIL propeller or its slipstream is influencing the adjacent propeller and its slipstream.

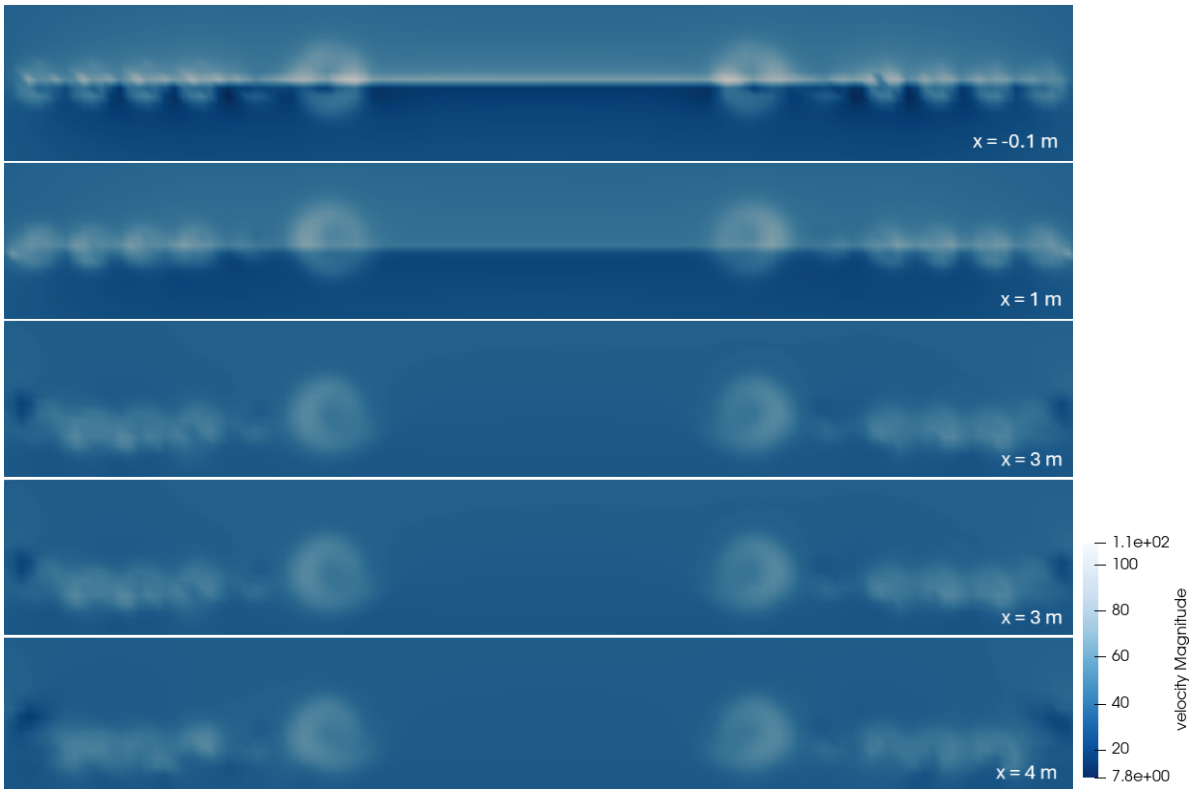

Figure 5.10: Flow field velocity analysis at different stations along the x axis.

5.3.5 Discussion

After obtaining and analyzing all results the entire picture of what was aimed for in the beginning of the research has finally come together. Only now it can be seen what decisions along the way were good and which were not. In the beginning it was very difficult to predict how each individual piece of this optimization would come together and if it would even work

in the end. In this section the main findings of the research will be discussed and the main conclusions drawn.

Firstly, let's discuss the answers to the set research questions. The first subquestion focused on the influence of positions and number of propellers on the performance of a DEP system. In chapter 4 an analysis of aircraft take-off velocity and angle of attack was made for different propeller configurations. The key takeaways are that increasing the number of lift augmenting propellers does in fact contribute to a reduction in take-off velocity and angle of attack, however the biggest difference is observed when going from one to two lift-augmenting propellers on each side of the wing. Lift-augmentation is also increased, however less so at higher angles of attack.

The next important observation is connected to the propeller inclination angle. It influences two major, however opposing effect, namely the increase in the local inflow angle of attack of the wing and the direction of the thrust vector. The interplay between these two was found to be related to the specific configuration and operational settings, both here and by other researchers. It is speculated, that in cases of higher thrust coefficients, higher angles of attack and relatively smaller wings and with shallower lift curve slopes, increasing propeller inclination angle would still have a negative effect on the wing lift coefficient, however it would have an overall positive effect on the effective lift coefficient. Analogously, the opposite would be true for lower thrust coefficients, lower angles of attack and larger wings with steeper lift curve slopes. Therefore, it can not be stated with certainty whether it is better to angle the propellers up or down, because it depends on the specific configuration and operational settings. However, it can be said that the effect of thrust component in the direction of lift should not be overlooked. Perhaps, because of this, it could actually be better not to use lift augmenting propellers, because similar to how they increase the wing lift coefficient, they would likely also decrease it more when pointed upwards, alongside also producing less lift than the minimum induced loss counterparts. However, this is only speculation and would require further research.

The vertical offset of the propellers was also found to have an effect on the take-off angle of attack and velocity, however it should be selected after selecting the propeller inclination angle. It appears that there is a much narrower range of values that would be beneficial for the lift augmentation and it largely depends on how the slipstream of the propeller intersects with the wing. Again, this is a complex problem and depends on the specific configuration and operational settings. It is a function of angle of attack, propeller inclination, slipstream deflection (function of propeller thrust coefficient) and forward offset of the propeller. From the aerodynamical point of view, it is usually better to have the propeller slightly above the wing, however the final decision should be made after considering all of the above mentioned factors.

By comparing the evaluated DEP configuration with a traditional aircraft configuration (same wing, one propeller on each side) there are a couple benefits to using a DEP system. Firstly, the take-off velocity and/or angle of attack are reduced, which could potentially lead to a shorter take-off distance. This can be inferred from figure 4.3, comparing different number of propellers with identical propeller disk area and consuming same amount of power (resulted in roughly the same amount of thrust). Of course by not having the entire span of the wing covered by many propellers they can be larger and more efficient, however this presents new challenges in terms of structural problems and high tip Mach numbers. Secondly, by having dedicated lift-augmenting and cruise propellers they can be designed for their specific purpose, which

could potentially lead to a more efficient system. During cruise, when the need for thrust and lift is lower only one of the propellers could be operational, producing thrust more efficiently than propellers, which also need do produce a lot of thrust during take-off. Furthermore, by placing them closer to the tips of the wing, the tip losses are reduced, which could potentially lead to a more efficient system. The dedicate cruise MIL propeller could also be designed with noise pollution in mind with less compromises, making the aircraft more environmentally friendly. The last advantage being mentioned is of course the added redundancy. However, it has to be noted that the DEP system is more complex and would require more maintenance, higher development and manufacturing costs and would likely be heavier than a traditional aircraft. Unfortunately, it would be too complex to analyze all of these factors in this research in the available time frame.

One potential problem, which was not yet discussed, is the excess thrust of the DEP system during landing. As discussed by Patterson (2016), aircraft equipped with DEP systems would likely have smaller wings, which by themselves would not produce enough lift to support the aircraft during landing. This would mean that the propellers would have to be used to augment lift during landing, which would also result in a decent amount of forward thrust. This is of course unwanted during the landing phase, since higher approach velocity results in bigger landing distance and higher kinetic energy that needs to be dissipated in case of an accident. This is in fact a big problem, which was in part addressed by Patterson, however it had to be skipped in the present work due to the complexity of the problem and the lack of time. A few potential solutions could be to use a deployable device during landing that would increase the drag of the aircraft but would not decrease its lift. Another option would be to utilize recuperation on certain propellers, which would convert the excess kinetic energy into electrical energy, but this is only feasible if there is enough lift produced by the wing and the active propellers.

Some thought should also be given to the feasibility of the low-fidelity models used in this research. Because optimizations usually evaluate numerous solutions the objective function needs to execute fairly quickly (if the computation resources are scarce). For this reason it was decided to utilize some fairly basic models, such as the blade element momentum theory, the lifting line method and de Young's method to predict the behavior of a slipstream of a propeller slipstream at an incidence with free stream flow. Furthermore, because of the complexity of the tackled problem, some assumptions and approximations had to be made in order to simplify it. One of the most difficult parts of this research project was finding the balance between accuracy and complexity, since including more accurate models and corrections would better predict the physical phenomena, but on the other hand it would increase the development and execution time, which were fairly limited. In hindsight, it would have been better to use more computing power which would allow for more complex models to be used or at least some assumptions to be relaxed. For example, the utilization of Trefftz plane based lifting line solver or a vortex lattice solver would likely produce more accurate results. Furthermore, the approximations made about the take-off procedure in the optimization cases were too simplistic and resulted in, to a certain degree, inaccurate absolute objective values, even though the relative differences between the solutions should be representable. All in all, for the given resources, the models used were deemed sufficient and sometimes produced surprisingly accurate results, however in the future it would be better to use more complex models and to relax some of the assumptions made.

Lastly, some attention should also be given to the optimization set-up, since it was found to be quite challenging and one of the main reasons, why this project took longer than expected. The selected problem is quite complex, especially because of the number of selected optimization variables and the chosen constraints. Because of the latter, the range of feasible solutions in the entire design space is very narrow, which made finding them quite challenging. If the bounds of the optimization variables were set too wide, the optimization algorithms sometimes wouldn't find feasible solutions at all, so they had to be set quite narrowly. This meant that sometimes the solutions on the pareto front would tend towards one of the extremities, so the bounds had to be adjusted and a long optimization case had to be rerun. At the concept earlier stages of research it was decided that it makes most sense that lift and drag are constraints, which makes them as narrow as the allowable margin. From the problem setup point of view this makes sense, however it makes the optimization problem much harder to solve. In the future, it would be a good idea to rethink the problem setup and to maybe use a different approach, which would relax the constraints and allow for a wider range of feasible solutions. This way the optimization algorithms would have a better chance of finding the pareto front and explore it in more detail.

6

Conclusions and Recommendations

6.1 Conclusions

This thesis focused on analyzing various installation geometries of Distributed Electric Propulsion (DEP) systems and assessing how changes in the number, position, and geometry of propellers affect aerodynamic and propulsive performance. To achieve this, a low-fidelity DEP analysis and optimization tool was developed in collaboration with Pipistrel Vertical Solutions. The tool takes selected input parameters and applies multi-objective optimization to identify configurations that perform well in both climb and cruise conditions. Throughout its development, the effects of individual parameters were evaluated and compared to findings in existing literature. In the final stage, the accuracy of the tool was benchmarked against a mid-fidelity simulation method.

The first key comparison was conducted between Minimum Induced Loss (MIL) and Lift-Augmenting (LA) propellers. It was confirmed that LA propellers generate a more uniform axial velocity profile in their slipstream, which—according to theory—enhances lift augmentation over the wing. Additionally, at higher loading conditions (lower advance ratios), LA propellers were shown to produce greater average axial velocity than MIL propellers, which maintain a flatter $U_{ax,avg}(J)$ curve and are more efficient across a wider range of operating conditions.

Subsequent analysis focused on the influence of the number of LA propellers, their inclination angles, and vertical offsets on take-off performance. As expected, increasing the number of LA propellers—while keeping the total disk area and power constant—resulted in shorter take-off distances by reducing induced drag and improving lift augmentation. The largest gains were seen when increasing from one to two propellers, with diminishing returns beyond that. It was also observed that the lift-augmenting effect decreases at higher wing angles of attack, as the wing approaches the peak of its lift curve. Propeller inclination was found to strongly influence total system lift; however, the optimal angle depended on a trade-off between the propeller-induced local angle of attack and the vertical component of thrust. Under high loading, such as during take-off, a slight upward inclination improved performance due to the added vertical thrust component. Finally, the vertical offset of the propellers also played a role, with maximum lift augmentation occurring when the propellers were positioned approximately $0.2R$ above the wing.

These insights were integrated into a multi-objective optimization framework aimed at minimizing take-off distance and maximizing cruise efficiency. The results confirmed and extended the trends observed in earlier sections. A variable correlation study highlighted the relationships between input variables and objectives. Among the configurations studied, the design with a tip-mounted MIL propeller performed best in cruise due to reduced wingtip vortex strength. In contrast, the tail-mounted MIL propeller configuration showed the weakest performance, lacking both lift augmentation and induced drag reduction during cruise.

Finally, the suitability of the low-fidelity models used in this study was assessed. A comparison between the developed tool and a mid-fidelity solver showed good agreement, validating the approach. Nevertheless, based on the experience gained, several avenues for improving both accuracy and computational efficiency of the tool were identified and are recommended for future development.

6.2 Recommendations for Future Research

While this study concentrated on the aerodynamic and propulsive performance of a Unifier19-type aircraft, this represents only a subset of the considerations required in the early stages of Distributed Electric Propulsion (DEP) aircraft design. Several avenues are proposed for future work to expand upon the current findings:

1. **Stability and Control Analysis**
   Future research should investigate the aerodynamic stability and controllability of DEP configurations. Since the performance of up- or down-pointing propellers was found to depend on the system configuration and flight regime, this characteristic could potentially be exploited to assist with pitch control. For instance, incorporating both up- and down-tilted propellers on each side of the wing could enable active pitch modulation, potentially reducing the size and complexity of horizontal control surfaces.
2. **Integration of Additional Disciplines**
   To move toward a more comprehensive aircraft design framework, further studies could integrate additional aspects such as structural analysis, weight estimation, battery sizing, and system-level constraints. These could be incorporated into a multidisciplinary design optimization (MDO) framework to explore more holistic and realistic trade-offs between competing objectives.
3. **Surrogate Modeling Using Higher-Fidelity Tools**
   A valuable extension of this work would be to construct a surrogate model of a similar DEP configuration using a mid-fidelity tool such as *DUST*. Comparing its predictions with those of the current low-fidelity model could help validate or refine the assumptions made, and highlight where additional accuracy may be warranted.
4. **Joint Wing and Propeller Optimization**
   Lastly, future work could explore simultaneous optimization of wing and propeller geometry. Jointly tailoring these components to one another would provide a more realistic representation of the coupled aerodynamic system and could lead to more optimal configurations than those found when optimizing the DEP system in isolation.

These proposed directions would contribute to a more complete understanding of DEP aircraft

performance and further enhance the tools available for their design and optimization.

References

Alba, C., Elham, A., German, B. J., & Veldhuis, L. L. L. M. (2018). A surrogate-based multi-disciplinary design optimization framework modeling wing–propeller interaction. *Aerospace Science and Technology*, *78*, 721–733. https://doi.org/10.1016/j.ast.2018.05.002

Aminaei, H., Mostofizadeh, A., & Dehghan Manshadi, M. (2019). Experimental and numerical study of wing boundary layer behavior in propeller flowfield. *Journal of Visualization*, *22*(3), 489–503. https://doi.org/10.1007/s12650-019-00553-w

Anderson, J. (2010). *Fundamentals of aerodynamics*. McGraw-Hill Education. https://books.google.si/books?id=xwY8PgAACAAJ

Baldoino, W. M., & Bodstein, G. C. R. (2004). Comparative analysis of the extended lifting-line theory to the classical lifting-line theory for finite wings.

Betz, A. (1919). Schraubenpropeller mit geringstem energieverlust. mit einem zusatz von l. prandtl. *Nachrichten von der Gesellschaft der Wissenschaften zu Göttingen, Mathematisch-Physikalische Klasse*, *1919*, 193–217. Retrieved February 12, 2025, from https://eudml.org/doc/59049

Chandrasekaran, B. (1986). *Method for the prediction of the installation aerodynamics of a propfan at subsonic speeds: User manual* (NAS 1.26:178057). Retrieved August 29, 2024, from https://ntrs.nasa.gov/citations/19860010889

Chow, F., Krause, E., Liu, C. H., & Mao, J. (1970). Numerical investigations of an airfoil in a nonuniform stream. *Journal of Aircraft*, *7*(6), 531–537. https://doi.org/10.2514/3.44208

Cole, J., Maughmer, M., & Bramesfeld, G. (2013, January 5). Aerodynamic design considerations for tiltrotor wing extensions and winglets. In *51st AIAA aerospace sciences meeting including the new horizons forum and aerospace exposition*. American Institute of Aeronautics; Astronautics. https://doi.org/10.2514/6.2013-1088

Conway, J. T. (1995). Analytical solutions for the actuator disk with variable radial distribution of load. *Journal of Fluid Mechanics*, *297*, 327–355. https://doi.org/10.1017/S0022112095003120

Conway, J. T. (1998). Exact actuator disk solutions for non-uniform heavy loading and slipstream contraction. *Journal of Fluid Mechanics*, *365*, 235–267. https://doi.org/10.1017/S0022112098001372

De Young, J. (1965). Propeller at high incidence [Publisher: American Institute of Aeronautics and Astronautics]. *Journal of Aircraft*, *2*(3), 241–250. https://doi.org/10.2514/3.43646

Deb, K., Pratap, A., Agarwal, S., & Meyarivan, T. (2002). A fast and elitist multiobjective genetic algorithm: NSGA-II [Conference Name: IEEE Transactions on Evolutionary Computation]. *IEEE Transactions on Evolutionary Computation*, *6*(2), 182–197. https://doi.org/10.1109/4235.996017

Devinant, P. (1998). An approach for unsteady lifting-line time-marching numerical computation. *International Journal for Numerical Methods in Fluids*, *26*(2), 177–197. https://doi.org/10.1002/(sici)1097-0363(19980130)26:2<177::aid-fld633>3.0.co;2-p

Drela, M. (1989). XFOIL: An analysis and design system for low reynolds number airfoils. In T. J. Mueller (Ed.), *Low reynolds number aerodynamics*. Springer. https://doi.org/10.1007/978-3-642-84010-4_1

Drela, M. (2006). QPROP formulation. Retrieved May 23, 2024, from https://web.mit.edu/drela/Public/web/qprop/qprop_theory.pdf

Epema, K. (2017). Wing optimisation for tractor propeller configurations: Validation and application of low-order numerical models adapted to include propeller-induced velocities. Retrieved March 18, 2024, from https://repository.tudelft.nl/islandora/object/uuid%3Ab091880e-7a0a-423c-a11e-6afe9b9575e3

Fei, X., German, B., & Patterson, M. D. (2018, January 7). Exploring the effects of installation geometry in high-lift propeller systems. In *2018 AIAA aerospace sciences meeting*. American Institute of Aeronautics; Astronautics. https://doi.org/10.2514/6.2018-0277

Glauert, H. (1983). *The elements of aerofoil and airscrew theory*. Cambridge University Press. https://doi.org/10.1017/CBO9780511574481

Goldstein, S., & Prandtl, L. (1929). On the vortex theory of screw propellers [Publisher: Royal Society]. *Proceedings of the Royal Society of London. Series A, Containing Papers of a Mathematical and Physical Character*, *123*(792), 440–465. https://doi.org/10.1098/rspa.1929.0078

Heidelberg, L., & Woodward, R. (1987, October 19). Advanced turboprop wing installation effects measured by unsteady blade pressure and noise. In *11th aeroacoustics conference*. American Institute of Aeronautics; Astronautics. https://doi.org/10.2514/6.1987-2719

Hess, J. L., & Smith, A. M. O. (1967). Calculation of potential flow about arbitrary bodies. *Progress in Aerospace Sciences*, *8*, 1–138. https://doi.org/10.1016/0376-0421(67)90003-6

Jameson, A. (1970). The analysis of wing-propeller flow interaction. http://aero-comlab.stanford.edu/Papers/jameson_nasa-228_1969.pdf

Kennedy, J., & Eberhart, R. (1995). Particle swarm optimization. *Proceedings of ICNN'95 - International Conference on Neural Networks*, *4*, 1942–1948 vol.4. https://doi.org/10.1109/ICNN.1995.488968

Khan, W., & Nahon, M. (2015). Development and validation of a propeller slipstream model for unmanned aerial vehicles [Publisher: American Institute of Aeronautics and Astronautics]. *Journal of Aircraft*, *52*(6), 1985–1994. https://doi.org/10.2514/1.C033118

Kroo, I. (1986). Propeller-wing integration for minimum induced loss [Publisher: American Institute of Aeronautics and Astronautics _eprint: https://doi.org/10.2514/3.45344]. *Journal of Aircraft*, *23*(7), 561–565. https://doi.org/10.2514/3.45344

Larrabee, E. E. (1979). Practical design of minimum induced loss propellers [Publisher: SAE International]. *SAE Transactions*, *88*, 2053–2062. Retrieved October 8, 2024, from http://www.jstor.org.tudelft.idm.oclc.org/stable/44699041

Larrabee, E. E., & French, S. E. (1983). Minimum induced loss windmills and propellers. *Journal of Wind Engineering and Industrial Aerodynamics*, *15*(1), 317–327. https://doi.org/10.1016/0167-6105(83)90201-5

Leng, Y., Yoo, H., Jardin, T., Bronz, M., & Moschetta, J.-M. (2019, January 6). Aerodynamic modeling of propeller forces and moments at high angle of incidence. In *AIAA scitech 2019 forum*. American Institute of Aeronautics; Astronautics. https://doi.org/10.2514/6.2019-1332

Metcalfe, M. (1985, July 8). On the modelling of a fully-relaxed propeller slipstream. In *21st joint propulsion conference*. American Institute of Aeronautics; Astronautics. https://doi.org/10.2514/6.1985-1262

Miranda, L., & Brennan, J. (1986, June 9). Aerodynamic effects of wingtip-mounted propellers and turbines. In *4th applied aerodynamics conference*. American Institute of Aeronautics; Astronautics. https://doi.org/10.2514/6.1986-1802

Munk, M. M. (1909). *Isoperimetrische aufgaben aus der theorie des fluges* [Doctoral dissertation]. Retrieved February 10, 2025, from https://vdoc.pub/documents/isoperimetrische-aufgaben-aus-der-theorie-des-fluges-1opbqkonoh5g

Munk, M. M. (1923, January 1). General theory of thin wing sections. Retrieved February 10, 2025, from https://ntrs.nasa.gov/citations/19930091206

Nebro, A., Durillo, J., Garcia-Nieto, J., Coello Coello, C., Luna, F., & Alba, E. (2009). SMPSO: A new PSO-based metaheuristic for multi-objective optimization. *2009 IEEE Symposium on Computational Intelligence in Multi-Criteria Decision-Making(MCDM)*, 66–73. https://doi.org/10.1109/MCDM.2009.4938830

Niro, C., Savino, A., Cocco, A., & Zanotti, A. (2024). Mid-fidelity numerical approach for the investigation of wing-propeller aerodynamic interaction. *Aerospace Science and Technology*, *146*, 108950. https://doi.org/10.1016/j.ast.2024.108950

Patterson, M. D. (2016). Conceptual design of high-lift propeller systems for small electric aircraft [Publisher: Georgia Institute of Technology]. Retrieved March 25, 2024, from http://hdl.handle.net/1853/55569

Prandtl, L. (1923, January 1). *Applications of modern hydrodynamics to aeronautics* (NACA-TR-116) (NTRS Author Affiliations: Goettingen Univ. NTRS Document ID: 19930091180 NTRS Research Center: Legacy CDMS (CDMS)). Retrieved September 17, 2024, from https://ntrs.nasa.gov/citations/19930091180

Ribner, H. S. (1945, January 1). Propellers in yaw [NTRS Author Affiliations: NTRS Report/Patent Number: NACA-TR-820 NTRS Document ID: 19930091897 NTRS Research Center: Legacy CDMS (CDMS)]. Retrieved February 12, 2025, from https://ntrs.nasa.gov/citations/19930091897

Savino, A., Ferreri, A., & Zanotti, A. (2024). Validation of a mid-fidelity numerical approach for wind turbine aerodynamics characterization [Number: 7 Publisher: Multidisciplinary Digital Publishing Institute]. *Energies*, *17*(7), 1517. https://doi.org/10.3390/en17071517

Silverstein, A., & Wilson, H. A. (1939, August 1). Drag and propulsive characteristics of air-cooled engine-nacelle installations for large airplanes, special report [NTRS Author Affiliations: National Advisory Committee for Aeronautics. Langley Aeronautical Lab. NTRS Report/Patent Number: NACA-SR-122 NTRS Document ID: 20090014207 NTRS Research Center: Legacy CDMS (CDMS)]. Retrieved October 11, 2024, from https://ntrs.nasa.gov/citations/20090014207

Sinnige, T. (2018). *Aerodynamic and aeroacoustic interaction effects for tip-mounted propellers: An experimental study* [Doctoral dissertation, Delft University of Technology]. https://doi.org/10.4233/UUID:214E1E9A-C53E-47C7-A12C-B1EB3EC8293B

Sørensen, J. N., & Shen, W. Z. (2002). Numerical modeling of wind turbine wakes [_eprint: https://asmedigitalcollection.asme.org/fluidsengineering/article-pdf/124/2/393/5678518/393_1.pdf]. *Journal of Fluids Engineering*, *124*(2), 393–399. https://doi.org/10.1115/1.1471361

Takallu, M., & Gentry, J., G. (1992, January 6). Aerodynamic characteristics of a propeller powered high lift semispan wing. In *30th aerospace sciences meeting and exhibit*. American Institute of Aeronautics; Astronautics. https://doi.org/10.2514/6.1992-388

Unifier19. (n.d.). Papers and project material. Retrieved October 16, 2024, from https://www.unifier19.eu/www.unifier19.eu/index5508.html?page_id=245

Veldhuis, L. L. M. (2005). Propeller wing aerodynamic interference. Retrieved March 12, 2024, from https://repository.tudelft.nl/islandora/object/uuid%3A8ffbde9c-b483-40de-90e0-97095202fbe3

Viterna, L. A., & Corrigan, R. D. (1982). Fixed pitch rotor performance of large horizontal axis wind turbines [NTRS Author Affiliations: NASA Lewis Research Center NTRS Document ID: 19830010962 NTRS Research Center: Legacy CDMS (CDMS)]. Retrieved February 17, 2025, from https://ntrs.nasa.gov/citations/19830010962

Wang, Q., Jiang, Z., & Zhang, Q. (2014). Regionalized actuator disk model designed by optimization method for propeller slipstream computation [Publisher: Taylor & Francis _eprint: https://doi.org/10.1080/19942060.2014.11015503]. *Engineering Applications of Computational Fluid Mechanics*, *8*(1), 127–139. https://doi.org/10.1080/19942060.2014.11015503

Weissinger, J. (1947, March 1). *The lift distribution of swept-back wings* (NACA-TM-1120) (NTRS Author Affiliations: National Advisory Committee for Aeronautics. Langley Aeronautical Lab. NTRS Document ID: 20030064148 NTRS Research Center: Langley Research Center (LaRC)). Retrieved February 10, 2025, from https://ntrs.nasa.gov/citations/20030064148

Wu, Y.-T., & Porté-Agel, F. (2011). Large-eddy simulation of wind-turbine wakes: Evaluation of turbine parametrisations [Company: Springer Distributor: Springer Institution: Springer Label: Springer Number: 3 Publisher: Springer Netherlands]. *Boundary-Layer Meteorology*, *138*(3), 345–366. https://doi.org/10.1007/s10546-010-9569-x

A

Optimization Case Setup

Parameter	Description	Value
N_{prop}	Number of LA propellers on one side of the wing	5
configuration	Position of the MIL propeller	inboard / outboard / tail
$U_{\infty,CR}$	Free stream velocity during cruise	80 m/s
a_{TO}	Acceleration of the aircraft during take-off	1.3 m/s^2
$\mathrm{m}_{\mathrm{aircraft}}$	Aircraft mass	7500 kg
b	Wing span	20 m
c	Wing chord (constant)	1.58 m
α_{TO}	Take-off angle of attack	10 deg
$\mathrm{airfoils}_{\mathrm{MIL,root}}$	Airfoil used for the MIL propeller	MH114
$\mathrm{airfoils}_{\mathrm{MIL,tip}}$	Airfoil used for the MIL propeller	MH117
$\mathrm{airfoils}_{\mathrm{LA,root}}$	Airfoil used for the LA propeller	MH114
$\mathrm{airfoils}_{\mathrm{LA,tip}}$	Airfoil used for the LA propeller	MH117
$\mathrm{airfoils}_{\mathrm{wing}}$	Airfoil used for the wing	Clark Y
x_{MIL}	Position of the MIL propeller	$0.4b/2$ (inboard), $0.9b/2$ (outboard)
$J_{MIL,TO}$	Advance ratio of the MIL propeller during take-off	0.75
$J_{MIL,CR}$	Advance ratio of the MIL propeller during cruise	1.0